Forest Ecology and Management 589 (2025) 122751

Contents lists available at ScienceDirect

Forest Ecology and Management

journal homepage: www.elsevier.com/locate/foreco

New allometric models for the USA create a shift in forest carbon estimation, modeling, and mapping

Lucas K. Johnson [a,b,*], Michael J. Mahoney [a], Grant M. Domke [c], Colin M. Beier [d]

[a] State University of New York College of Environmental Science and Forestry, Division of Environmental Science, Syracuse, NY, 13210, USA
[b] Oregon State University, College of Forestry, Corvallis, OR, 97331, USA
[c] USDA Forest Service, Northern Research Station, St. Paul, MN, 55108, USA
[d] State University of New York College of Environmental Science and Forestry, Department of Sustainable Resources Management, Syracuse, NY, 13210, USA

ARTICLE INFO

Keywords:
Aboveground biomass
National forest inventory
Forest inventory and analysis
Landsat
Design-based estimation
Model-based estimation

ABSTRACT

The United States national forest inventory (NFI) serves as the foundation for forest aboveground biomass (AGB) and carbon accounting across the nation. These data enable design-based estimates of forest carbon stocks and stock-changes at state and regional levels, but also serve as inputs to model-based approaches for characterizing forest carbon stocks and stock-changes at finer spatial and temporal resolutions. Although NFI tree and plot-level data are often treated as truth in these models, they are in fact estimates based on regional species-group models and parameters known collectively as the Component Ratio Method (CRM). In late 2023 the Forest Inventory and Analysis (FIA) program replaced CRM nationwide with a new National Scale Volume and Biomass Estimators (NSVB) system that offers more precise and accurate representations of forest AGB and carbon. Given the prevalence of model-based AGB studies relying on FIA, there is concern about the transferability of methods from CRM to NSVB models, as well as the comparability of existing CRM AGB products (e.g. maps) to new and forthcoming NSVB AGB products. To begin addressing these concerns we compared previously published CRM AGB maps and estimates to new maps and estimates produced using identical methods with NSVB AGB reference data. Our results suggest that models relying on passive satellite imagery (e.g. Landsat) provide acceptable estimates of point-in-time NSVB AGB and carbon stocks, but fail to accurately estimate growth in mature or closed-canopy forests. We highlight that existing estimates, models, and maps based on FIA reference data are no longer compatible with NSVB, and recommend new methods as well as updated models and maps for accommodating this shift. Our collective ability to adopt NSVB in our modeling and mapping workflows will help us provide the most accurate spatial forest carbon data possible in order to better inform local management and decision making.

1. Introduction

Measuring and monitoring forest biomass is an active area of research, with mapped predictions of forest aboveground biomass (AGB) in particular being used to inform carbon accounting efforts alongside other conservation and stewardship activities. In the United States (US) context, such maps often rely upon AGB estimates from the US Forest Inventory and Analysis program (FIA) which provides tree-level AGB estimates for millions of trees across thousands of plots throughout the US (Gray et al., 2012). These tree-level estimates can then be aggregated to plots and used to estimate AGB across the landscape (Bechtold and Patterson, 2005). However, these design-based estimates are limited to a relatively coarse spatial resolution due to the density of the FIA sample (McRoberts, 2011). A plethora of studies have demonstrated that model-based estimation can produce AGB estimates at finer resolutions, fitting models to predict FIA's AGB estimates using remote sensing data products (for instance, Kennedy et al., 2018a; Johnson et al., 2022, 2023; Huang et al., 2019; Ayrey et al., 2021; Zheng et al., 2007). These studies commonly treat the AGB estimates provided by FIA as ground truth and adopt them with only minimal adjustments or corrections (if any).

However, FIA's AGB estimates are not actual ground truth measurements, but are instead produced by applying allometric models to variables (e.g. height, diameter at breast height) more easily measured in the field. Historically these estimates have been made using the component ratio method [CRM; Woodall et al. (2011b); Heath

* Corresponding author at: Oregon State University, College of Forestry, Corvallis, OR, 97331, USA.
E-mail addresses: johnsl27@oregonstate.edu (L.K. Johnson), mjmahone@esf.edu (M.J. Mahoney), grant.m.domke@usda.gov (G.M. Domke), cbeier@esf.edu (C.M. Beier).

https://doi.org/10.1016/j.foreco.2025.122751
Received 27 December 2024; Received in revised form 15 April 2025; Accepted 18 April 2025
Available online 21 May 2025

et al. (2009)], a combination of regional species-group-specific allometric models that estimate biomass as a function of tree diameter and height. Although AGB estimates from CRM are useful, they do have several limitations. In particular, CRM models for non-merchantable portions of trees were not fit using actual tree component measurements (e.g. branches, tops, foliage) and the administrative boundaries used to delineate regional models did not correspond to underlying ecological gradients (Woodall et al., 2011b; Westfall et al., 2023).

In light of these limitations and the rapidly growing interest in measuring and monitoring AGB and forest carbon stocks, FIA introduced a new National Scale Volume and Biomass Estimators (NSVB) system to replace CRM nationwide in late 2023 (Westfall et al., 2023). NSVB estimates of AGB address several concerns with CRM and provide a more unified and accurate set of estimates for AGB across the nation (Westfall et al., 2023). NSVB also represents a step-change in forest AGB estimation, with NSVB estimating 14.6% more forest AGB nationwide than CRM estimates using the same field measurements. This difference varies across geographic regions and forest compositions with differences in estimated state-level AGB ranging from +37.1% for Indiana to −1.5% for Washington (Westfall et al., 2023; Virginia Tech, 2023a,c). A major driver of these differences appears to be improvements to the estimation of top and limb biomass, and as a result species that are poor self-pruners or otherwise grow denser tops and branches often saw the largest increases in estimated AGB under NSVB.

The new AGB and carbon estimates introduced with NSVB do not reflect on-the-ground changes in forest structure or function, but simply represent accounting changes resulting from swapping one system of allometric models for another. Although they are purely due to structural differences in the allometric models used, these accounting changes aim to improve our understanding of forest AGB and carbon stocks and fluxes across the landscape by increasing the precision and accuracy of tree-level volume, biomass, and carbon estimates. Therefore it is necessary to update existing carbon-monitoring systems that rely on FIA estimates of AGB or carbon to incorporate the benefits of NSVB in resulting map products and estimates. However, given the importance of top and limb biomass in NSVB estimates, it is not clear if common model-based approaches relying on remotely sensed data, which may have difficulty penetrating the canopy to capture the density of tops and branches in a forest, will be as effective at predicting NSVB estimates. This in turn has obvious downstream implications for how forest carbon accounting will be impacted by the shift from CRM to NSVB estimates of forest AGB and carbon stocks, and suggests the urgent need to revisit existing modeling pipelines. Further, we are concerned about the comparability of existing maps produced using CRM AGB to newer products produced using NSVB AGB. It is not yet known whether AGB maps produced using NSVB will be simple "rescalings" of their CRM equivalents, or if these new maps will exhibit new patterns across focal landscapes. These questions and concerns are particularly pressing given the proliferation of AGB models based on FIA data (for instance, Kennedy et al., 2018a; Johnson et al., 2022, 2023; Huang et al., 2019; Ayrey et al., 2021; Zheng et al., 2007) and both the growing demand and technical capacity for remote monitoring of forest carbon stocks.

To begin answering these questions, we compared previously published CRM AGB maps to new maps produced using identical methods but NSVB AGB estimates as reference data. Specifically, we replicated the methodology of Johnson et al. (2023) which was developed to map CRM AGB at a 30 m resolution annually (1990–2019) for a variety of applications related to map-based stock-change assessments, screening or prioritizing forest parcels for enrollment in nature-based climate programs, and future monitoring, reporting, and verification (MRV) systems across New York State (NYS). With this modeling framework in place, we saw an opportunity to explore the impacts of exchanging CRM AGB reference data for NSVB AGB reference in a well-established empirical modeling approach relying on FIA plots and Landsat imagery (Lu, 2006; Hall et al., 2006; Powell et al., 2010; Pflugmacher et al., 2012; Deo et al., 2016; Kennedy et al., 2018a). We (1) produced four NYS-wide NSVB AGB maps for 2005, 2010, 2015, and 2019; (2) compared estimates of statewide CRM and NSVB AGB stock and stock-changes across these four years; (3) compared CRM and NSVB AGB maps and the spatial patterns of their differences for 2019; and (4) compared the ability for machine learning models based on Landsat imagery to estimate CRM and NSVB AGB overall. Given the estimated 5.7% increase in NYS AGB following a transition to NSVB (Virginia Tech, 2023b) and the increased accuracy in NSVB tree biomass (Westfall et al., 2023), we expected Landsat-based models of NSVB-AGB to produce larger predictions on average, yielding larger statewide totals, and stronger agreement with FIA reference data and estimates.

2. Methods

2.1. Study area

New York State covers 141,297 km^2 of the northeastern United States. Daily temperatures across the state ranged from -17 °C to 28 °C in 2019, while monthly precipitation for the same period ranged from 5.0 cm to 16.8 cm (NOAA National Centers for Environmental Information, 2022). Elevation ranges from −2 m to 1584 m above sea level (US Geological Survey, 2019). The majority of the state occupies the northern hardwoods-hemlock forest region, though there are important inclusions of beech-maple-basswood and Appalachian oak communities in the western and southern reaches of the state, respectively (Dyer, 2006). Like much of the US Northeast, NYS was extensively deforested during the 18th and 19th centuries, with subsequent reforestation and conservation resulting in a landscape dominated by forest stands that are now over 100 years old (Whitney, 1994; Lorimer, 2001; Mahoney et al., 2022b). NYS created the Forest Preserve in 1885, establishing the foundation for what became the Adirondack and Catskill Parks decades later. Any state-owned or acquired lands within these parks has since been designated as 'forever wild' and has largely been preserved, with no timber harvesting.

The US Forest Service estimates that National Scale Volume and Biomass estimators (NSVB) induced changes to aboveground biomass (AGB) estimates for New York State (NYS) will be moderate, with an estimated 5.7% increase in AGB statewide (Virginia Tech, 2023b). This increase is not distributed evenly across species, however; FIA estimates that red spruce (*Picea rubens*) AGB will increase by approximately 38.7%, while sugar maple (*Acer saccharum*) AGB will increase by just under 5%, and yellow birch (*Betula alleghaniensis*) AGB will decrease by roughly 5% (Virginia Tech, 2023b). These species are not uniformly distributed throughout the state: red spruce is most common in high-elevation forests throughout the Adirondack Park; sugar maple is the largest contributor to statewide total standing biomass (Virginia Tech, 2023b) with the greatest abundance in montane regions with more mature forests, often in combination with yellow birch (Wilson et al., 2012; Riemann et al., 2014). As a result, it is not yet known how local to regional estimates of forest AGB and carbon sequestration will be impacted by the switch to NSVB.

2.2. Comparing CRM and NSVB AGB for individual trees

In light of the larger statewide AGB estimates, the increased accuracy and magnitude of estimates of biomass stored in tops and limbs of trees, and the variability of these changes across tree species associated with a shift to NSVB (Westfall et al., 2023; Virginia Tech, 2023b), we compared FIA estimates of tree-level AGB, and top and branch biomass, for the Component Ratio Method (CRM) and NSVB. These comparisons aimed to provide more insight into the main drivers of the difference in predictions and estimates at pixel to statewide scales. Specifically, we selected the twelve most abundant species by stem count in our model development dataset (Section 2.3.1; 78% of the population) and plotted the difference between NSVB and CRM estimates as a function of tree-diameter for each species.

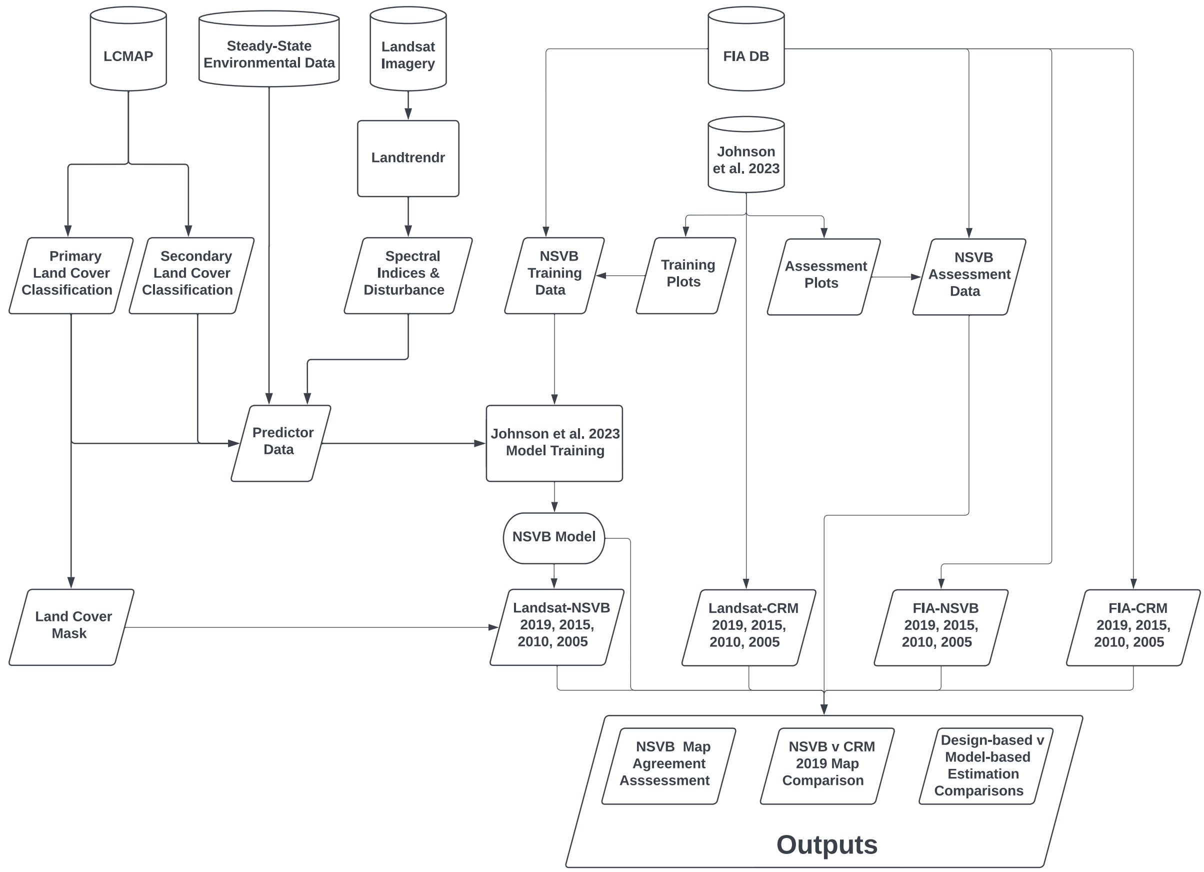

Fig. 1. A flowchart diagram showing the key elements of both the modeling and mapping methodology and the CRM v NSVB comparisons. Cylinders represent data repositories, parallelograms represent data products and results, rectangles represent processing steps, and ovals represent models.

2.3. Modeling NSVB AGB

The "direct" modeling approach developed in Johnson et al. (2023) used CRM AGB estimates at FIA field plots as reference data and temporally matching Landsat imagery and landcover classifications, as well as temporally static climate, topographic, and ecological layers as predictor data. The resulting machine learning ensemble model was used to make annual (1990–2019) CRM AGB predictions at a 30 m resolution across NYS. We repeated the methods used in the direct modeling approach from Johnson et al. (2023) to develop four NSVB AGB maps (2005, 2010, 2015, 2019) for NYS. We emphasize that the same plots (model-development and map assessment), auxiliary data, and machine learning algorithms were used; the only difference is in the allometric models used to generate plot-level AGB reference data from the FIA database. We summarize how we used the Johnson et al. (2023) direct modeling approach to make NSVB maps and estimates and how we compare them to CRM maps and estimates below (Fig. 1).

2.3.1. Field inventory data

Each FIA plot contains four 7.32 m radius (24 ft) circular subplots, one at the center of the plot and three centered 36.6 m (120 ft) away from the plot center at azimuths of 120°, 240°, and 360° (Bechtold and Patterson, 2005). We obtained true plot centroids for FIA plots within New York State under an agreement with the FIA program office. Plots are assigned to one of five panels, each assumed to have complete spatial coverage across the state, and remeasured on a 5–7 year basis. Trees on land considered to be forested within each subplot ≥ 2.54 cm (1 in) DBH are measured and translated to estimates of AGB using the NSVB system of allometric models. To maintain consistency with CRM and Johnson et al. (2023), we aggregated AGB estimates for trees ≥ 12.7 cm (5 in) to the FIA plot-level. We then area-normalized these estimates to convert them into units of Mg ha^{-1}. FIA considers land to be forested if an area at least 0.4 ha in size and 120 m in width is not developed for nonforest land uses and is at least 10% stocked with trees. Under this definition, it is likely that some woody AGB exists on some of these nonforest lands not measured by FIA. However, in the absence of field measurements for these areas, we treated these nonforest lands as having no AGB.

We filtered the complete set of FIA plots within New York State measured between 2002 and 2019 to only those inventories where all four subplots were measured. This initial selection criteria resulted in a pool of 5144 plots. We then divided this set of plots into model development and map assessment datasets using FIA's panel designation, with one of the five panels randomly selected and all plots with this designation assigned to the map assessment dataset, and the remaining plots assigned to the model development dataset. In this way we partitioned 20% of the available data for an independent map assessment, yielding a probability sample with complete spatial coverage which allowed us to use design-unbiased estimators for map agreement metrics (Riemann et al., 2010; Stehman and Foody, 2019).

We then filtered the model development set to only include completely forested (and therefore completely measured) plots. We added to this set a group of completely nonforested plots with maximum LiDAR-derived canopy heights ≤ 1 m, which we assumed to correspond to having 0 AGB (Johnson et al., 2022), resulting in a total of 2049 model development plots inventoried between 2002 and 2019. The map assessment set was further filtered to remove plots external to our mapped area based on our landcover mask (Johnson et al., 2023), resulting in 545 assessment plots inventoried in 2007, 2012, 2018, and

2019. When plots in model development or map assessment sets were inventoried more than once, single instances were randomly selected so that each plot was associated with only one inventory year.

2.3.2. Auxiliary data

Following Mahoney et al. (2022b), we derived a set of 16 predictors from annual (2002–2019) growing-season medoid composites of Landsat collection 1 imagery (USGS, 2018) using coefficients from Roy et al. (2016). These predictors were then processed using Landtrendr in Google Earth Engine using normalized burn ratio (NBR) vertices to produce temporally segmented, gap-filled, and smoothed timeseries metrics (Kennedy et al., 2010, 2018b). Derived metrics included NBR (Kauth and Thomas, 1976), tasseled-cap wetness, brightness, and greenness (Cocke et al., 2005), normalized difference vegetation index (Kriegler et al., 1969), simple ratio (Jordan, 1969), and modified simple ratio (Chen, 1996), as well as the one-year change at each pixel for each of these indices. We use the spectral module for Google Earth Engine for index calculation (Montero et al., 2022). We additionally used the Landtrendr NBR segmentation to identify the years since the most recent disturbance as well as the associated magnitude of change in NBR at each pixel for the temporal range of 1985–2019.

To this set of auxiliary data we added annual primary and secondary land cover classifications from the US Geological Survey's Land Change Monitoring, Assessment and Projection (LCMAP) version 1.2 (Zhu and Woodcock, 2014; Brown et al., 2020) and a set of steady-state variables including 30 year normals for precipitation and temperature (PRISM Climate Group, 2022), elevation, aspect, slope, and topographic wetness index derived from a 30 m digital elevation model (Beven and Kirkby, 1979; US Geological Survey, 2019; Mahoney et al., 2022a), predictions from a global canopy height model (Simard et al., 2011), distance to nearest waterbodies identified by the US Census Bureau (US Census Bureau, 2013; Walker, 2023), National Wetland Inventory classifications from the US Fish and Wildlife Service, and the Environmental Protection Agency's level 4 ecozones (Omernik and Griffith, 2014; CEC, 1997). Ecozones were aggregated to their corresponding level 3 ecozone if they did not cover ≥ 2% of the state. If the aggregated level 3 ecozones also did not cover ≥ 2% of the state, they were assigned an ecozone of "other".

All auxiliary data was projected to match Landsat 30 m pixel geometries using the terra package (Hijmans, 2023) for the R programming language (R Core Team, 2023). We used the exactextractr library (Baston, 2022) to spatially associate FIA plot inventories (both model-development and map-assessment sets described in Section 2.3.1) with temporally matching gridded auxiliary data. We calculated the mean of pixel values intersecting with subplot locations weighted by the fraction of each pixel overlapping with the plot area.

2.3.3. Model fitting

We further partitioned the model development dataset (described in Section 2.3.1) into a training set (80% of observations) and a testing set (20% of observations). We fit a random forest (RF) as implemented in the ranger R package (Breiman, 2001; Wright and Ziegler, 2017), a gradient boosting machine (GBM) as implemented in the lightgbm R package (Friedman, 2002; Ke et al., 2017; Shi et al., 2022), and a support vector machine (SVM) as implemented in the kernlab R package (Cortes and Vapnik, 1995; Karatzoglou et al., 2004) to this training set. Hyperparameters were selected for each method through an iterative grid search using five-fold cross-validation. More information on this tuning procedure is available in Section 2.6 (Model development) of Johnson et al. (2023).

We then used five-fold cross-validation to generate predictions from each of these models, using their optimal hyperparameters identified through the grid search, for each observation in the training dataset. We then ensembled the three base models (RF, GBM, SVM) in order to produce a single final prediction by fitting a linear regression model estimating FIA plot AGB as a function of each of the base model predictions (Wolpert, 1992; Dormann et al., 2018). We selected this ensemble as our final model and all further discussions of model predictions refer to this ensemble. Following Johnson et al. (2023), and in order to avoid redundant comparisons between models of NSVB and CRM AGB, we focused here on the map agreement assessment and have provided model testing set metrics separately in Supplementary Materials 1.

2.3.4. Variable importance comparison

We conducted a variable importance assessment to investigate the degree to which relationships between auxiliary data layers and FIA plot-level AGB would change under a shift to NSVB. Variable importance was computed for the linear ensemble model using a permutation approach (Breiman, 2001). Since many of our predictors are highly correlated, we first clustered them based on Spearman rank correlation Euclidean distances. A cluster dendrogram was used to identify 16 distinct variable clusters. For each p predictor, a separate linear ensemble model is trained. The pth predictor is selected, and all other predictors in the pth predictor's cluster are excluded. A single predictor from the remaining 15 clusters is selected. The values for the pth predictor are then shuffled, breaking any potential relationship between the pth predictor and the response (AGB). The model is then trained with these 16 predictors (following the approach in Section Section 2.3.3), and RMSE is assessed via 10-fold-cross-validation on the 80% model development partition. Variable importance is then computed as the delta RMSE from the pth predictor model against the full model trained with all p predictors. The variable importances are then standardized, such that the sum of all p importance scores equals 1. In this analysis default hyperparameter values are used for all component ML models. We followed the same approach with CRM AGB reference data.

2.4. Mapping and postprocessing

We used the linear ensemble model to make predictions for all 30 m pixels across the state for 2019 (the most recent map year in Johnson et al. (2023)), 2015, 2010, and 2005 (the earliest year possible to produce a statewide design-based estimate from the public FIA database.) All downstream results and comparisons were made with predictions from the linear ensemble model. Following Johnson et al. (2023), we masked our predictions with annual LCMAP version 1.2 primary landcover classification product to remove pixels classified as developed, cropland, water, and barren. We then compared these maps to CRM-based maps representing 2019, 2015, 2010, and 2005 from Johnson et al. (2023).

2.5. Map agreement assessment

As this study represents one of the first model-based estimation studies based on NSVB AGB, we perform a comprehensive map agreement assessment of our NSVB AGB model following methods described in Riemann et al. (2010). Using the ensemble model, we predicted AGB at each 30 m pixel coincident with FIA plots in the map assessment set (Section 2.3.1), using predictors derived from Landsat imagery from the same year as each FIA plot inventory. We then used the exactextractr library to calculate the mean of these pixel predictions at each plot, weighted by the fraction of each pixel overlapping with the plot area (Baston, 2022). This data was pooled together across years (2007, 2012, 2018, 2019) resulting in a temporally generalized agreement assessment.

Following Riemann et al. (2010) we estimated model assessment metrics both directly using these weighted averages and FIA plot-level estimates (plot-to-pixel) and after aggregating predictions and FIA plot-level estimates to multiple regular grids of variably-sized hexagons, increasing in size such that hexagon centroids ranged from 2 km to 50 km apart (1 km separation yields the equivalent to a plot-to-pixel comparison).

Model assessment metrics included root mean squared error (RMSE; Eq. (1)), mean absolute error (MAE; Eq. (2)), mean error (ME; Eq. (3)), and R^2 (Eq. (4)):

$$RMSE = \sqrt{(\frac{1}{n})\sum_{i=1}^{n}(y_i - \hat{y}_i)^2} \tag{1}$$

$$MAE = (\frac{1}{n})\sum_{i=1}^{n}|y_i - \hat{y}_i| \tag{2}$$

$$ME = (\frac{1}{n})\sum_{i=1}^{n} y_i - \hat{y}_i \tag{3}$$

$$R^2 = 1 - \frac{\sum_{i=1}^{n}\left(y_i - \hat{y}_i\right)^2}{\sum_{i=1}^{n}\left(y_i - \bar{y}\right)^2} \tag{4}$$

Where y_i is FIA estimated AGB, $\hat{y}_i$ is model-predicted AGB, and $\bar{y}$ is mean FIA estimated AGB. Interpreting RMSE and MAE can be difficult, as these metrics are in units of Mg ha^{-1} which can make interpret the relative magnitude of errors challenging without also knowing the mean and distribution of pixel AGB values. To aid interpretation, we present normalized variants of these metrics rescaled by the mean AGB within the map assessment dataset:

$$RMSE\ \% = 100 \cdot \frac{RMSE}{\bar{y}} \tag{5}$$

$$MAE\ \% = 100 \cdot \frac{MAE}{\bar{y}} \tag{6}$$

Each of these metrics was estimated at a plot-to-pixel scale and after aggregation to each grid of hexagons. Metric calculations used the waywiser and yardstick R packages (Mahoney, 2023; Kuhn et al., 2023). For the plot-to-pixel scale, we additionally produced a 1:1 scatter plot to examine where over- or under-predictions of FIA reference data occurred. We included the same metrics produced in Johnson et al. (2023) to be able to compare agreement with FIA across NSVB AGB maps and models produced in this study to CRM analogs. Finally, we assessed how well the distribution of predictions from Landsat-based models of CRM and NSVB AGB approximated the distributions of their corresponding FIA estimates within the map assessment set using empirical cumulative distribution function plots and Kolmogorov–Smirnov (KS) tests (Massey, 1951).

2.6. Map comparisons

We directly compared a 2019 NSVB AGB map produced in this study to a 2019 CRM AGB map produced by the direct modeling approach in Johnson et al. (2023). We also compared NSVB and CRM AGB percent rank maps representing each pixels position in the statewide distribution of biomass predictions (e.g. 100% rank is the largest prediction in the NYS map). We differenced AGB maps and percent rank maps to identify spatial patterns of both absolute changes between CRM and NSVB predictions as well as shifts relative to the statewide distributions. We also assessed the agreement between these 2019 AGB maps across multiple scales of aggregation with variably-sized hexagons (centroids 1 km to 50 km apart; Section 2.5; Riemann et al. (2010)) using the agreement coefficient (AC; Eq. (7)) from Ji and Gallo (2006):

$$AC = 1 - \frac{\sum_{i=1}^{n}\left(\hat{y}_i - y_i\right)^2}{\sum_{i=1}^{n}\left(|\bar{\hat{y}} - \bar{y}| + |\hat{y}_i - \bar{\hat{y}}|\right)\left(|\bar{\hat{y}} - \bar{y}| + |y_i - \bar{y}|\right)} \tag{7}$$

Here y represents predictions from the CRM model, while $\hat{y}$ represents predictions from the NSVB model. AC is a symmetrical metric which allows for errors in both y and $\hat{y}$, making it useful to compare model predictions to one another. AC is bounded $[-\infty, 1]$, with a value of 1 representing perfect agreement.

A benefit of AC is that it can be broken down into systematic (AC_s) and unsystematic (AC_u) components so that we were able to determine the degree to which differences in maps produced using CRM AGB are systematically different from maps produced using NSVB AGB, and therefore the degree to which they could be linearly rescaled to match NSVB-based estimates. Further details of this derivation and the decomposition of AC into AC_s and AC_u are provided in Ji and Gallo (2006) and Supplementary Materials 2.

We tested rescaling model-based CRM AGB to model-based NSVB AGB with a simple linear regression model as follows:

$$NSVB_{mod} = \beta_0 + \beta_1 \cdot CRM_{mod} + \beta_2 \cdot Elevation + \varepsilon \tag{8}$$

Where $NSVB_{mod}$, CRM_{mod}, and Elevation were pixel-level values sampled from a raster stack containing maps of NSVB and CRM AGB (2019; Mg ha^{-1}) and elevation (m) as layers. We randomly divided the 1,000,000 pixel sample into training (80%; n = 800,000) and testing (20%; n = 200,000) sets for model fitting and assessment respectively.

2.7. Statewide stock estimates

We additionally compared estimates of statewide AGB stocks across both sets of estimation methods (design-based vs model-based approaches) and allometric models (CRM vs NSVB). We made design-based estimates of total NYS AGB and aboveground carbon (AGC) stocks for both NSVB and CRM, and for the years 2005, 2010, 2015, and 2019 using FIA procedures as described in Pugh et al. (2018) and Bechtold and Patterson (2005). These procedures use the Horvitz–Thompson estimator (Horvitz and Thompson, 1952) and leverage a two-phased sampling design that reduces variance through stratification. Our estimates included stems 12.7 cm (5 inches) and up, correspond to all forest land in NYS, and are 'temporally indifferent' (TI) implying that they pool all measurement panels within an inventory cycle to create a larger periodic inventory (Stanke et al., 2020; Bechtold and Patterson, 2005). TI estimation is commonly used in FIA estimation tools (Doser et al., 2025; Miles, 2015) and trades more temporal smoothing for smaller variance. The measurement panels for each estimation year were organized as follows: 2019: 2013–2019, 2015: 2010–2015, 2010: 2005–2010, 2005: 2002–2005. We emphasize that the same sample and estimator were used to make each pair of design-based estimates (e.g. CRM 2019 and NSVB 2019); the only difference was the set of allometric models used to generate plot-level AGB reference data from the FIA database. We then estimated model-based AGB stocks for both the CRM and NSVB-based models by multiplying the statewide average pixel-level AGB density (Mg ha^{-1}) by the total mapped area in NYS (Section 2.4). Following CRM protocols described in Woodall et al. (2011b), AGC stocks were assumed to be 50% of AGB for all model-based CRM estimates. Under the new NSVB protocols described in Westfall et al. (2023), species-specific carbon fractions are used to convert AGB to AGC. We did not have access to a fine-resolution species map for NYS in our map years, but instead computed statewide carbon fractions for each respective map-year (2005, 2010, 2015, 2019) as an average of species-specific carbon fractions, weighted by each species' relative contribution to FIA's statewide AGB estimates. We used these fractions to convert model-based estimates of statewide total NSVB AGB to statewide total NSVB AGC. Hereafter, we use the FIA- prefix to denote design-based estimates, and the Landsat- prefix to denote model-based estimates. We thus compare the following four estimation approaches: FIA-CRM, Landsat-CRM, FIA-NSVB, and Landsat-NSVB.

2.8. Comparing stock-changes with NSVB and CRM

We computed statewide stock-change estimates by computing all pairwise differences of stocks (Section 2.7) across years (2019, 2015, 2010, and 2005) for each method (e.g. 2019 FIA-CRM AGB minus 2005

Table 1
NSVB and CRM AGB map agreement results (vs FIA) for select scales using the map assessment set of FIA plots. RMSE, MAE, ME in Mg ha^{-1}. Scale = distance between hexagon centroids in km; PPH = plots per hexagon; n = number of comparison units (plots or hexagons). All metrics as defined in Section 2.5.

Scale	n	PPH	Allometric	MAE	% MAE	RMSE	% RMSE	ME	R^2
Plot:Pixel	545		NSVB	47.25	36.01	60.33	45.97	−3.86	0.37
			CRM	41.20	34.10	52.31	43.29	−4.83	0.38
20 km	293	1.86	NSVB	39.82	30.03	52.66	39.72	−2.32	0.39
			CRM	35.02	28.68	45.49	37.25	−3.22	0.41
30 km	171	3.19	NSVB	35.85	26.99	48.28	36.34	−0.72	0.39
			CRM	31.46	25.77	41.13	33.69	−2.10	0.40
50 km	74	7.38	NSVB	28.24	20.93	38.87	28.81	3.39	0.44
			CRM	24.94	20.14	35.05	28.31	1.36	0.42

FIA-CRM AGB). This resulted in six distinct stock change estimates (2019– 2005, 2019–2010, 2015–2005, 2019–2015, 2015–2010, and 2010–2005) representing three time steps (14-year, 9/10-year, and 4/5-year) for each estimation approach and system of allometric models (FIA-CRM, Landsat-CRM, FIA-NSVB, Landsat-NSVB). Additionally, we compared pixel-level stock-changes by first computing stock change maps as 2019 AGB minus 2005 AGB for NSVB and CRM and then differencing these stock change maps (Δ NSVB - Δ CRM). We used this stock-change difference map to identify landscape patterns of differences in statewide stock-change estimates.

3. Results

3.1. Tree-level differences

For the twelve most abundant species by stem count in our model development dataset, we found that NSVB aboveground biomass (AGB) estimates were often larger than CRM AGB estimates, and the magnitude of these differences increased as a function of tree diameter (Fig. 2a). For the same trees, differences between NSVB and CRM top and branch biomass estimates were almost always positive (Paper birch [*Betula papyrifera*] the notable exception; Fig. 2b). Trends in these differences were mostly non-linear. Based on these results and previous reports (Westfall et al., 2023; Virginia Tech, 2023b), NSVB is often estimating more tree-level biomass, and most of this biomass is attributed to the tops and limbs of trees, a component that was previously underrepresented in model building datasets (Westfall et al., 2023; Woodall et al., 2011b). These differences increase with tree size (Fig. 2), and thus we can infer that as trees grow NSVB is attributing more biomass to the tops and limbs of trees.

3.2. NSVB map agreement assessment

Mapped AGB predictions from the NSVB model became increasingly accurate and exhibited stronger agreement with FIA estimates as aggregation unit size increased; % MAE decreased from 36.01 (agreement between FIA plots and pixel-level predictions) to 20.93% (agreement for hexagonal units spaced 50 km apart), % RMSE decreased from 45.97 to 28.81%, and R^2 increased from 0.37 to 0.44 (Table 1; Supplementary Materials 3). RMSE and MAE followed similar patterns. ME estimates were small across all scales of assessment and did not exhibit a monotonic improvement with aggregation (Table 1; Supplementary Materials 3).

3.3. NSVB vs CRM map

NSVB maps (Fig. 3) yielded marginally worse agreement with corresponding FIA estimates than their CRM counterparts across all scales of aggregation (Table 1; % MAE, % RMSE). CRM and NSVB AGB models approximated the distributions of their corresponding FIA estimates similarly (Supplementary Materials 4), but NSVB models appeared to be more impacted by saturation, a common issue when modeling forest structure with passive satellite imagery (Lu, 2005; Duncanson et al., 2010; Johnson et al., 2023) where models underpredict the largest reference observations (Fig. 4). Within the map assessment partition, Landsat-NSVB predicts a maximum value that is 58.68% of the FIA NSVB reference maximum, while Landsat-CRM predicts a maximum value that is 62.44% of the FIA CRM reference maximum. Kolmogorov–Smirnov statistics confirmed that CRM AGB models were only marginally better at approximating the corresponding FIA distribution (CRM 0.17; NSVB 0.18).

Table 2
Results of a regression model representing NSVB AGB model predictions (Mg ha^{-1}) as a function of CRM AGB model predictions (Mg ha^{-1}) and elevation (m).

	Coefficient	Standard error	t	p
Intercept	9.533	0.051	186.7	< 0.001
CRM AGB	1.135	< 0.001	3,282.9	< 0.001
Elevation	−0.023	< 0.001	−276.2	< 0.001

NSVB and CRM AGB maps agreed with one another across all scales of aggregation (AC > 0.9), but agreement decreased with increasing aggregation (Fig. 5). The majority of the disagreement was due to systematic differences between the maps (ACs). The AGB difference map showed that models of NSVB AGB produced larger estimates relative to models of CRM AGB across most of NYS, but produced smaller estimates concentrated in what appear to be the montane forests of the Adirondack and Catskill regions (Fig. 6a). In contrast to the AGB difference map, the percent rank difference map showed a more uniform pattern of downshifts and upshifts in percent rank across NYS, highlighting 'gaining' and 'losing' areas in terms of AGB density (more or less AGB relative to the rest of the state) with a shift to NSVB. High-elevation areas still contained the largest relative downshifts in percent rank from CRM to NSVB (Fig. 6b) indicating that models estimated these areas to be much less AGB-dense relative to the rest of NYS following a change from CRM to NSVB.

The linear regression model (Eq. (8)) used to rescale CRM AGB to NSVB AGB was accurate (RMSE 14.07, MAE 10.93, ME 0.02) and represented 93% (R^2) of the variability in the model-based NSVB predictions from the test set. The regression coefficients succinctly described the observed spatial patterns of differences between model-based CRM and NSVB AGB (Fig. 6), indicating that NSVB AGB would increase by ~1.14 Mg ha^{-1} with every unit increase in CRM AGB and elevation held constant, but that NSVB AGB would decrease by ~2 Mg ha^{-1} for every 100 m of elevation gained and CRM AGB held constant (Table 2; Supplementary Materials 5).

3.4. Statewide stock and stock-change comparison

Estimates of total NSVB AGB and AGC for NYS were substantially larger than corresponding CRM estimates for both the design-based

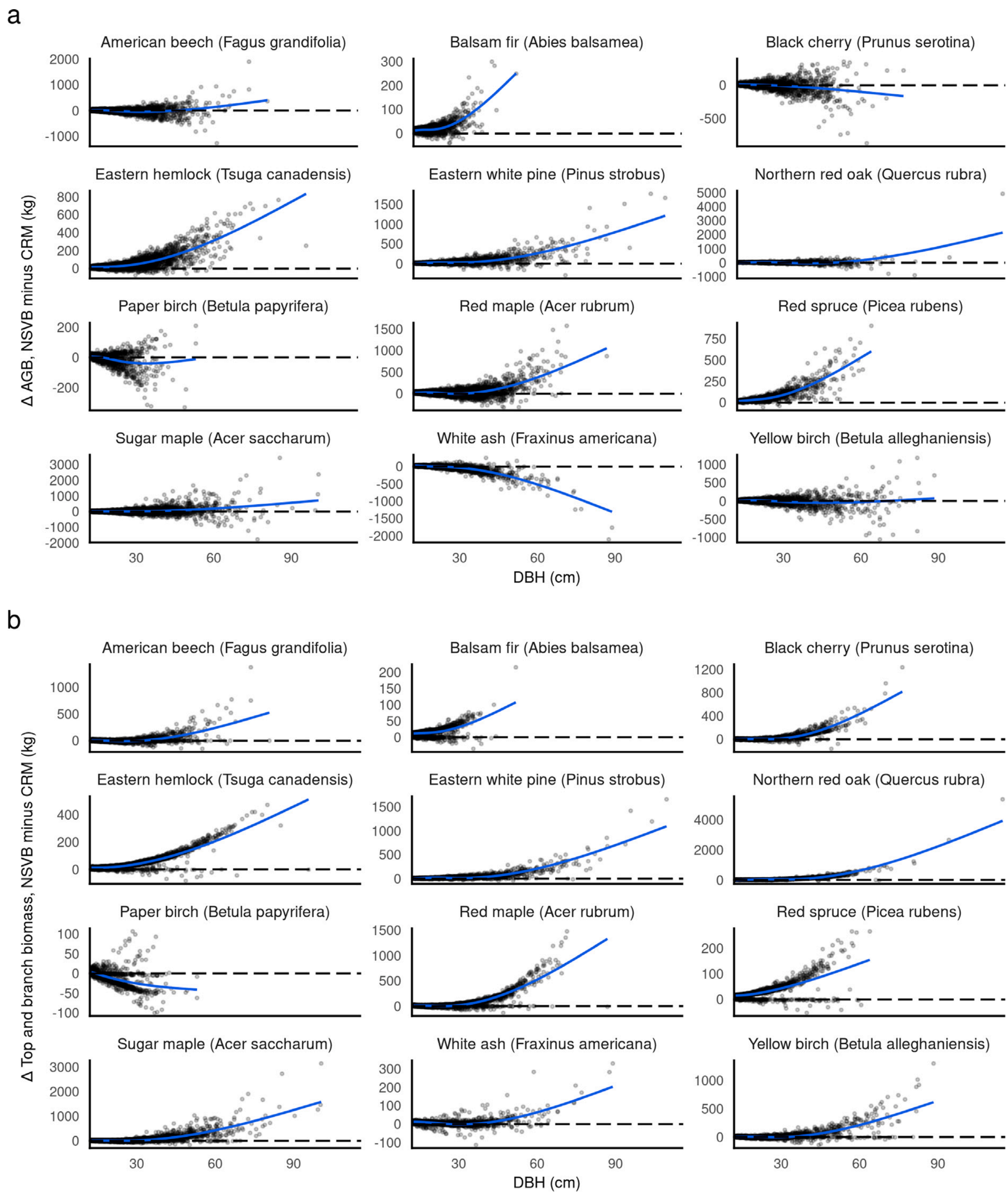

Fig. 2. (a) Tree-level AGB differences and (b) top and branches biomass differences as estimated by FIA (Δ biomass; NSVB minus CRM), as a function of diameter at breast height (DBH) partitioned by the 12 most abundant species in our model development dataset. Each point represents a single tree. Dashed horizontal lines represent matches of NSVB and CRM estimates. Blue lines are fit to data using cubic splines with two knots.

and model-based methods (Fig. 7). However, Landsat-CRM estimates were better aligned with FIA-CRM estimates. On average, Landsat-CRM stocks were ~2% larger than FIA-CRM stocks, but Landsat-NSVB stocks were ~10% large than FIA-NSVB stocks. Differences in carbon fractions applied to convert AGB to AGC appeared to have minimal impact on statewide stock agreement.

Although FIA-NSVB stock estimates were greater than FIA-CRM stock estimates, Landsat-NSVB stock-change estimates were smaller than their CRM counterparts (Fig. 8). This led to a greater disagreement between Landsat-NSVB and FIA-NSVB stock-change estimates. This was especially apparent for the 14-year timestep, where Landsat-NSVB underestimates FIA-NSVB estimates of 14-year statewide AGB accumulation by 55.21 MMT, whereas Landsat-CRM only underestimated FIA-CRM AGB stock-change by 7.58 MMT. Landsat-NSVB underestimation of FIA-NSVB stock-change estimates was present, but variable in magnitude, across all time steps. In particular, stock-changes where 2005 was the initial year yielded the largest disagreements, likely owing to the large disagreement between Landsat-NSVB and FIA-NSVB statewide AGB stock estimates in 2005 (Fig. 7). On the other hand, Landsat-CRM

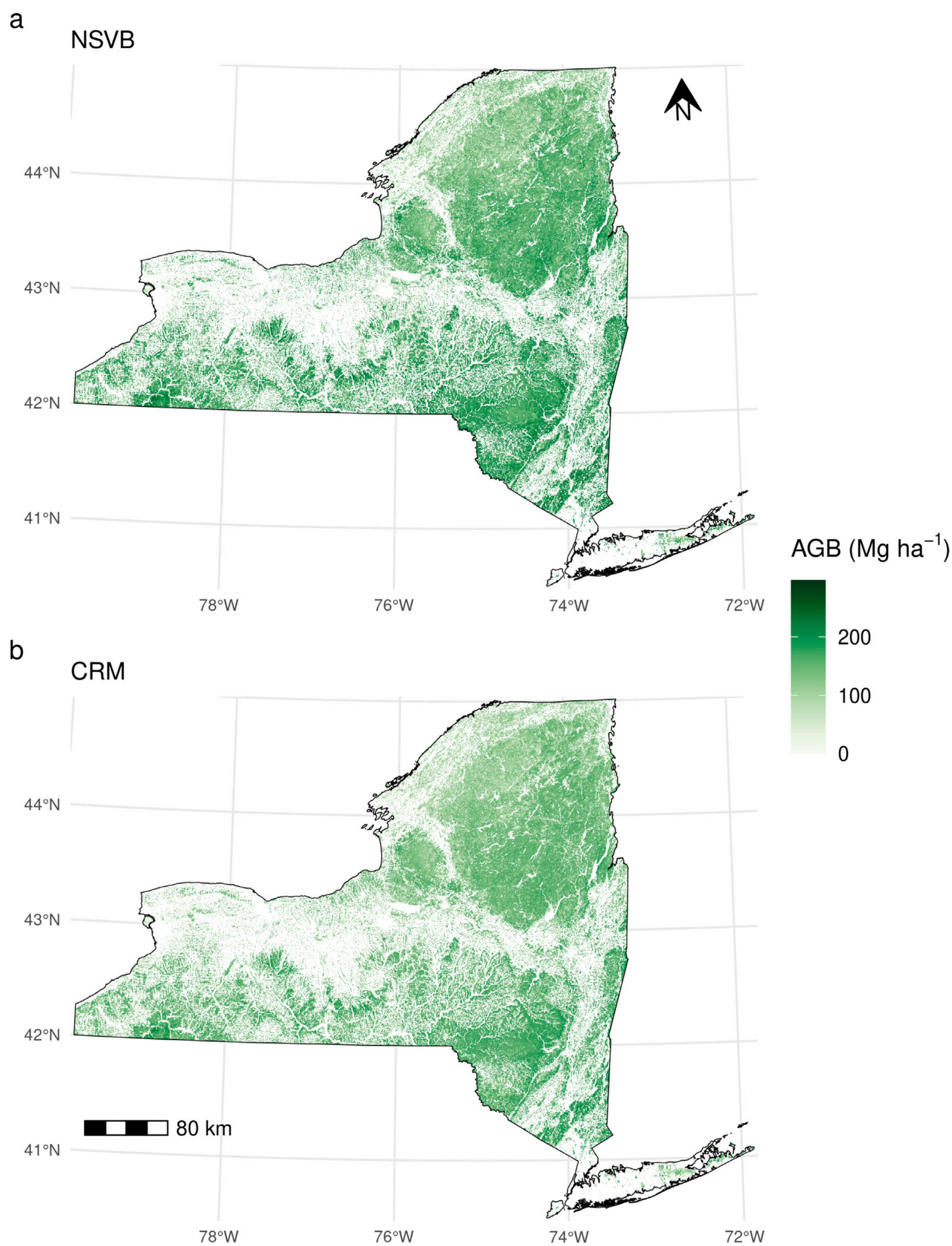

Fig. 3. Landsat-predicted AGB for 2019. (a) Predictions made with models trained on NSVB-based FIA reference data. (b) Predictions made with models trained on CRM-based FIA reference data.

variably under- and over-estimated FIA-CRM stock-changes across time steps.

The stock-change maps for NSVB and CRM yielded nearly identical spatial distributions of AGB losses and gains, however the magnitudes of losses and gains differed (Fig. 9a, b). AGB losses from 2005 to 2019 appeared to be greater in magnitude in the NSVB map than in the corresponding CRM map, particularly in the Adirondack region in the northeastern portion of the state (Fig. 9c). NSVB AGB gains over the time period were only marginally larger than corresponding CRM AGB gains throughout the south-central region, and along the southeastern border of the state.

3.5. Variable importance comparison

Variable importance shifts from Landsat-CRM to Landsat-NSVB were not readily interpretable or meaningful (Supplementary Materials 6).

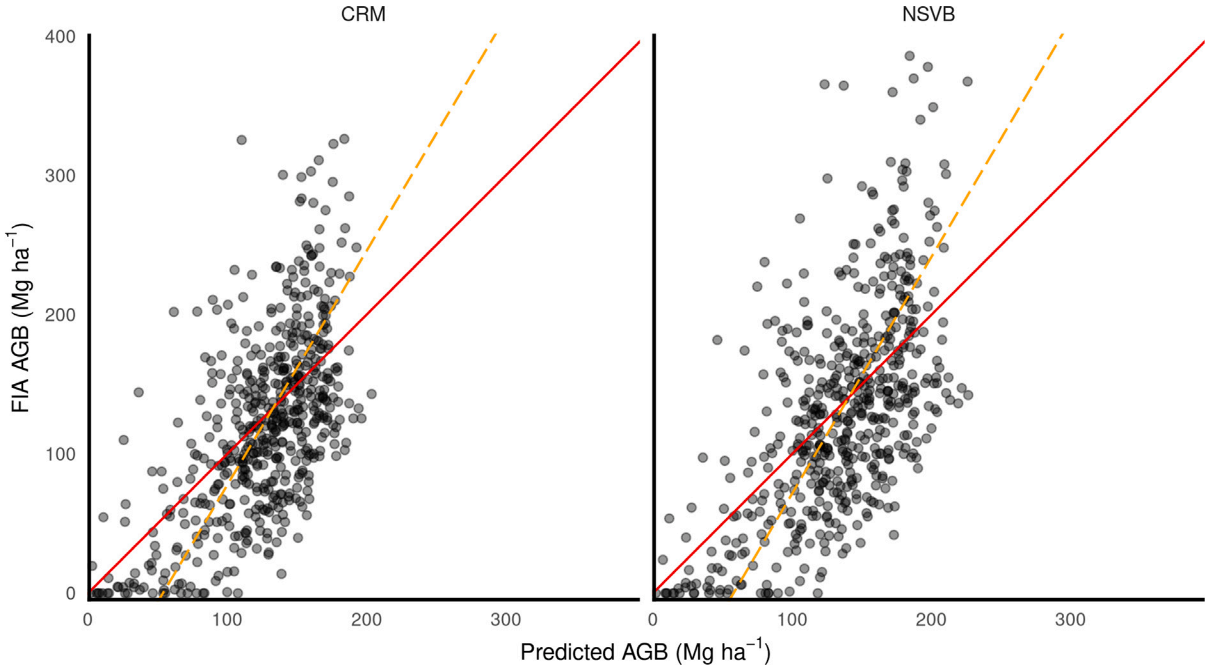

Fig. 4. Comparison of mapped AGB to FIA plot-level AGB for each set of allometric models (NSVB and CRM) for the map assessment set of FIA plots. Geometric mean functional relationship (GMFR) trend line shown with dashed (orange) line, and 1:1 line shown with solid (red) line.

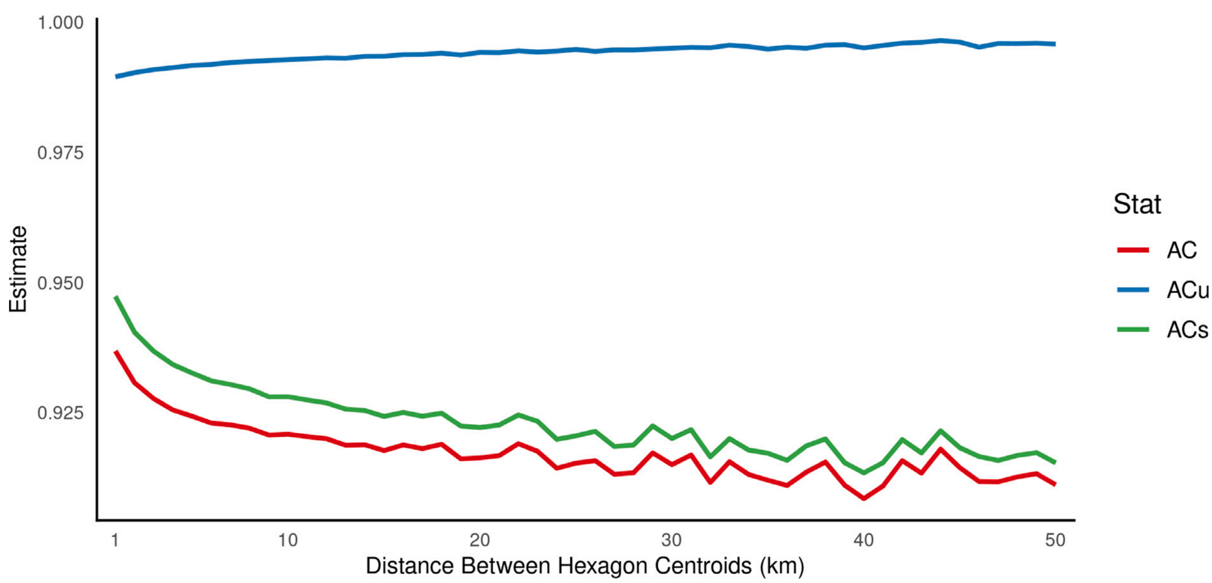

Fig. 5. Agreement between NSVB AGB maps and CRM AGB maps across scales represented by distances between hexagon centroids. AC (agreement coefficient) and its systematic (ACs) and unsystematic (ACu) components as defined in Section 2.5.

The maximum variable importance across both models (NSVB, CRM) was 0.031 and the largest change in importance across all variables was 0.0026 The largest rank shift among 58 variables was 11.

4. Discussion

In this study we investigated the transferability of well-established methods for estimating, modeling, and mapping aboveground biomass (AGB) based on Landsat imagery between two United States (US) Department of Agriculture Forest Inventory and Analysis (FIA) reference datasets constructed with different systems of allometric models: the legacy Component Ratio Method (CRM, Woodall et al., 2011a) and the new National Scale Volume and Biomass Estimators (NSVB, Westfall et al., 2023). To this end, we compared previously published CRM AGB maps and derived estimates (Johnson et al., 2023) to new maps and derived estimates produced using identical methods but with NSVB AGB reference data. We found that NSVB and CRM AGB maps agreed with one another, though systematic differences driven by NSVB allometric models were apparent in our maps; NSVB AGB predictions were generally larger than corresponding CRM AGB predictions and concentrations of smaller NSVB AGB existed in high-elevation regions of the state. Maps of NSVB and CRM AGB agreed similarly with

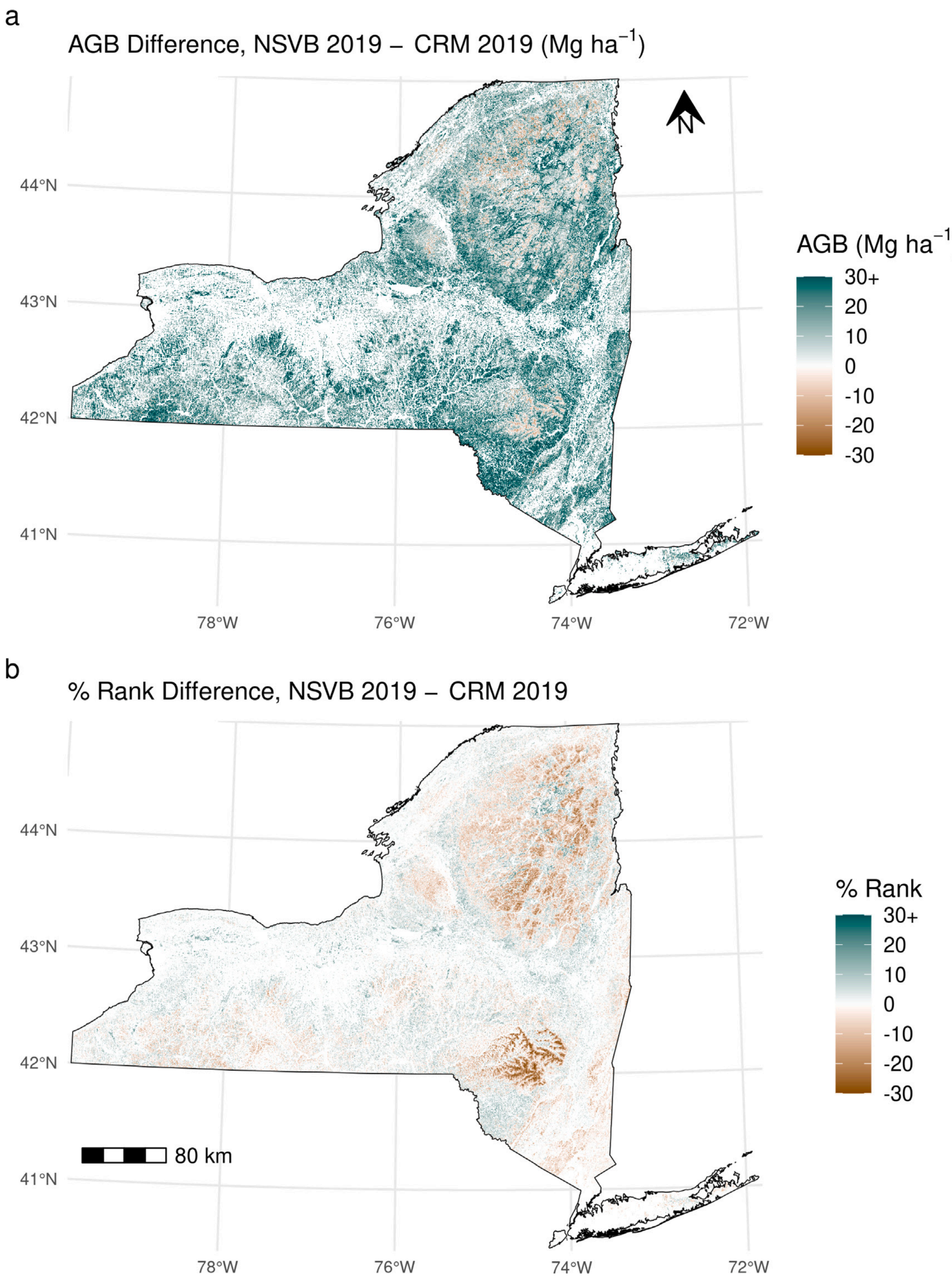

Fig. 6. Difference maps for 2019 computed as Landsat-predicted AGB with NSVB-based FIA reference data minus Landsat-predicted AGB with CRM-based FIA reference data. (a) AGB differences in units of Mg ha^{-1} (b) Percent rank differences. Mapped values capped at +/−30.

corresponding FIA reference datasets, however models of NSVB AGB were more impacted by saturation and thus were limited in their ability to characterize AGB growth statewide. These findings demonstrate that NSVB introduces a shift for model-based forest carbon estimation and monitoring in the US and suggest the need to update entire modeling pipelines, especially for applications that require the representation of forest growth over time. In particular, incorporating NSVB-based reference data in carbon monitoring systems may require updated models, careful comparisons with CRM-based estimates, and new modeling approaches including additional remotely sensed datasets such as LiDAR.

4.1. Comparing NSVB and CRM AGB maps

We interpreted that the differences between our NSVB and CRM AGB maps (Fig. 6) were driven by changes in the underlying system of allometric models, specifically how CRM and NSVB estimates differed

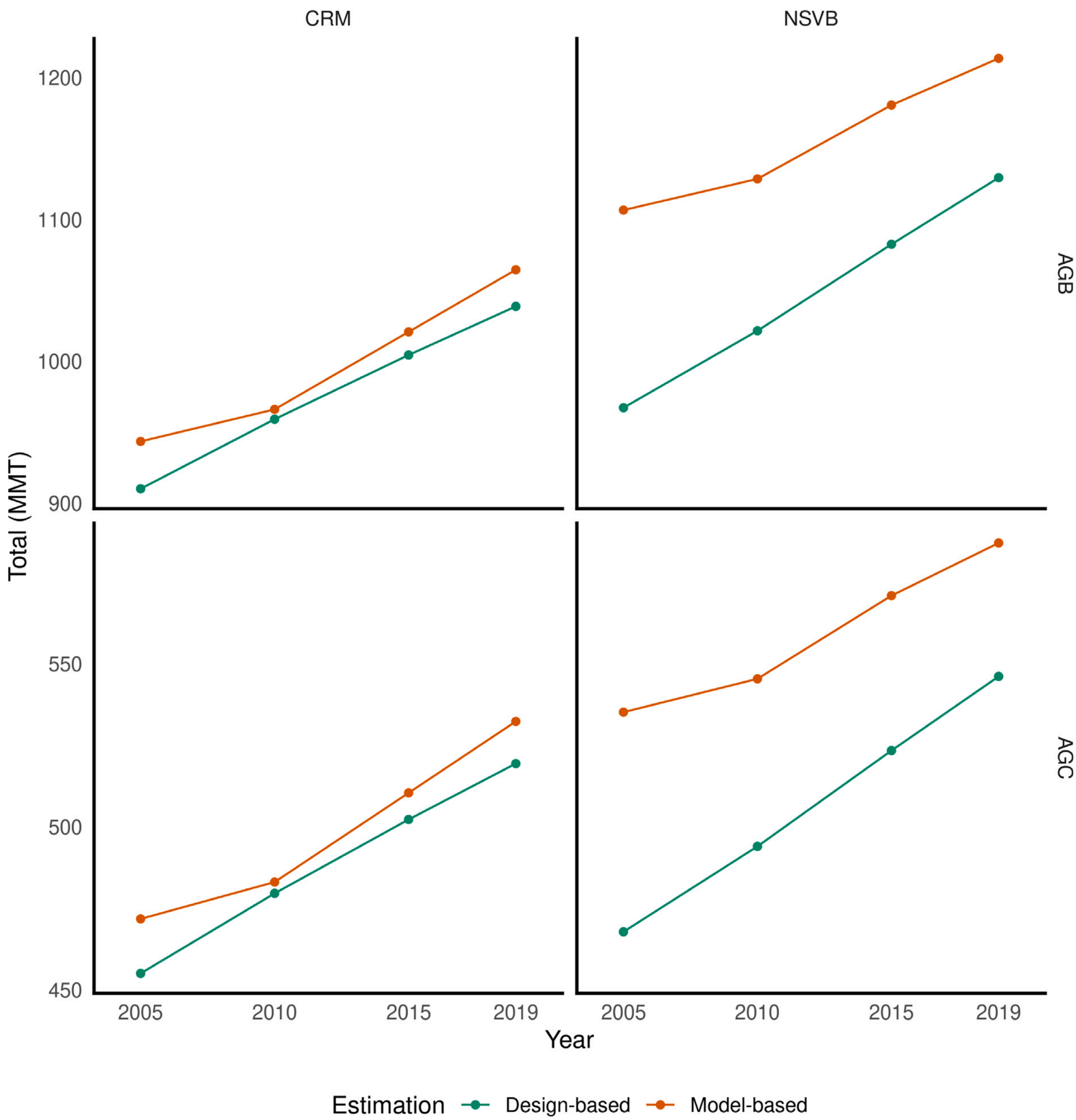

Fig. 7. Timeseries of statewide stocks (2005, 2010, 2015, 2019) for aboveground biomass (AGB) and aboveground carbon (AGC) by estimation method (model-based vs design-based) and allometric (CRM vs NSVB). Model-based and design-based procedures are held consistent and only the set of allometric models used to generate plot-level AGB reference data from the FIA database differ. Values in millions of metric tons.

for individual species and size classes (Fig. 2). NSVB was designed (in part) to yield more precise estimates of top and limb biomass and as a result, the majority of the differences between the estimates from the two systems can be attributed to these non-merchantable components of trees (Westfall et al., 2023; Virginia Tech, 2023b). Within NYS, an FIA estimated 57.5% increase in statewide top and limb biomass contributed to an overall 5.7% increase in total AGB (Virginia Tech, 2023b). This increase was generally reflected in our map differences where NSVB AGB model predictions were larger than corresponding CRM AGB predictions across most of the state. NSVB AGB increases relative to CRM AGB may be most pronounced for large-diameter individuals and for species that are poor self-pruners or otherwise grow densely-packed branches (Fig. 2; Westfall et al. (2023); Virginia Tech (2023b)). Conversely, trees in high-elevation areas where we observed smaller predictions of NSVB AGB relative to CRM AGB (Table 2; Fig. 6) often have smaller stems due to shallow soils and more stressful climates. Thus, it stands to reason that high-elevation forests generally would not see the same increase in top and branch biomass with the transition to NSVB as more size- and species-diverse forests throughout the state. These same montane regions contain large proportions of sugar maple and yellow birch (Wilson et al., 2012; Riemann et al., 2014) which were among the species that did not show large AGB increases associated with the transition to NSVB (Fig. 2; Virginia Tech (2023b)). These map differences exemplify the degree to which updates and improvements to allometric models may yield structural changes to downstream model-based estimates along relevant ecological gradients such as species composition, climate, and topography.

Although there were notable differences between maps (Fig. 6), statistical comparisons indicated strong agreement between NSVB and CRM AGB maps (Fig. 5). Agreement (AC, ACs) decreased as a function of aggregation unit size, indicating that differences were spatially clustered (particularly in the aforementioned high-elevation forests), and thus were amplified through aggregation. Across all scales of

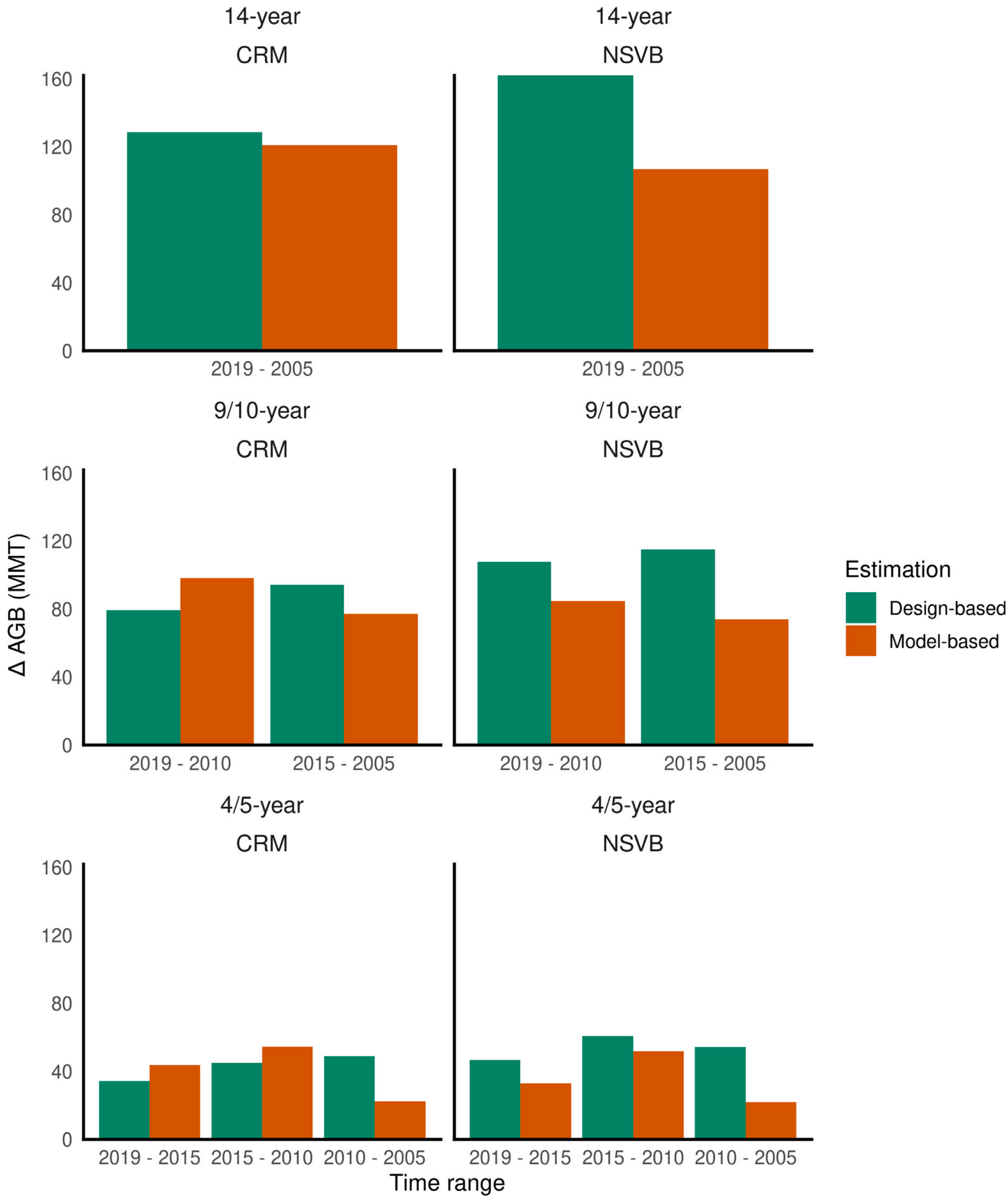

Fig. 8. Statewide stock-changes across 14- to 4-year timesteps for aboveground biomass (AGB) by estimation method (model-based vs design-based) and allometric (CRM vs NSVB). Model-based and design-based procedures are held consistent and only the set of allometric models used to generate plot-level AGB reference data from the FIA database differ. Values in millions of metric tons.

aggregation, most of the disagreement between mapped predictions was attributed to systematic differences, due to the relatively uniform increase in AGB under NSVB in most forested regions of the state. As a result, it was possible to translate existing CRM AGB estimates to their NSVB equivalents through relatively simple linear relationships (Table 2; Eq. (8)). However, any such adjustments outside the scope of this study will require further investigation, will likely be model- and task-specific, and should be performed with care given the spatial variability of NSVB-CRM differences.

4.2. Difficulty modeling NSVB AGB growth with passive remote sensing

While the relative increase in estimated stocks from FIA-CRM to FIA-NSVB where mirrored with model-based estimates, the relative decrease in estimated stock-changes from Landsat-CRM to Landsat-NSVB contradicted design-based estimates where FIA-NSVB stock-changes were larger than FIA-CRM stock-changes (Fig. 7; Fig. 8). This significantly widened the gap between design- and model-based stock-change estimates; Landsat-CRM estimates of statewide AGB change were only

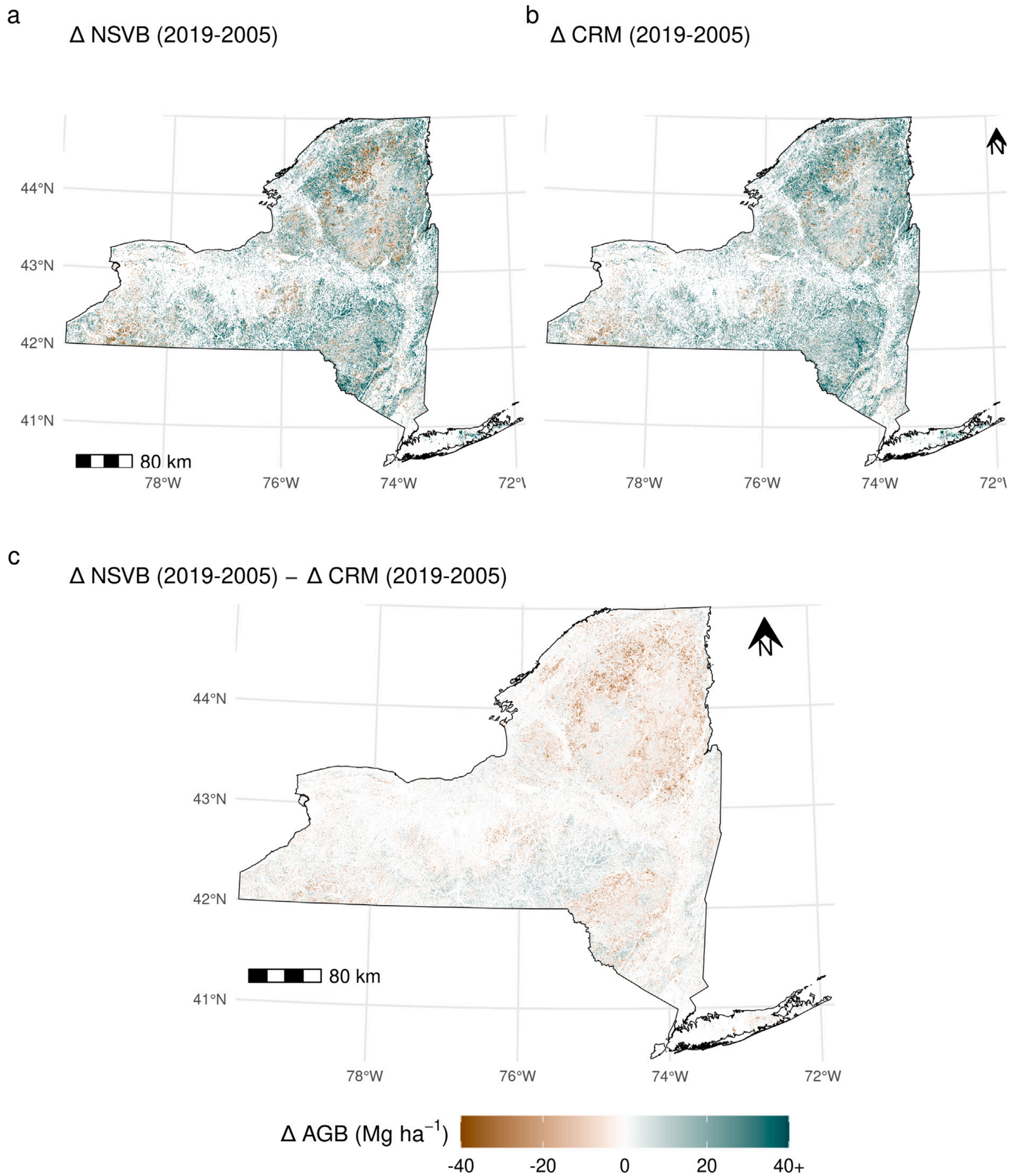

Fig. 9. Stock-change map comparison. (a) 15-year NSVB stock-change map (Δ NSVB; 2019 AGB - 2005 AGB). (b) 15-year CRM stock-change map (Δ CRM; 2019 AGB - 2005 AGB). (c) Stock-change difference map computed as Δ NSVB minus Δ CRM. Mapped values capped at +/−40 Mg ha^{-1}.

7.58 million metric tons less than FIA-CRM, but Landsat-NSVB estimates of statewide AGB change where 55.21 million metric tons less than FIA-NSVB. The introduction of species-specific carbon fractions with NSVB appeared to have minimal impact on aboveground carbon estimates relative to the impact of differences in AGB estimates.

We did find that NSVB AGB models fit using Landsat imagery were still able to generate acceptable point-in-time AGB stock estimates as evidenced by the comparable agreement with FIA-reference plots in our map agreement assessment (Table 1). Further, this study does not cast doubt on the ability of NSVB AGB models to detect discrete canopy changes driven by deforestation, reforestation, and disturbance events. However, under NSVB, a greater number of plots had AGB values beyond the saturation point for model predictions, indicating that Landsat-NSVB was less capable of accurately estimating AGB in denser forest stands with larger individual trees than Landsat-CRM (Fig. 4). This may be caused by the increased accuracy and magnitude of NSVB allometric model estimates for biomass attributed to the tops and limbs of trees (Westfall et al., 2023), particularly for larger-diameter trees (Fig. 2). Although Landsat-CRM was already impacted by saturation in forests with closed canopies (Johnson et al., 2023), we speculate that more accurate representation of tree branch biomass with NSVB allometries only exacerbates this issue; substantial additions of biomass and increased biomass variability beneath the canopy are likely difficult to "see from space".

Our results therefore suggest that passive remote sensing alone may not be capable of monitoring NSVB AGB growth through a stock-change approach. This may be especially true in regions similar to NYS and the much of the Northeastern US where historical land-use dynamics indicate that the majority of forest stands have either reached or are approaching maturity (Section 2.1). The inclusion of active remote sensing systems in NSVB modeling pipelines, including aerial and spaceborne LiDAR or synthetic aperture radar, may offer the only solutions to monitoring NSVB AGB growth at scale. These classes of sensors have the capacity to penetrate closed canopies and better represent structural attributes related to AGB, thus reducing saturation effects (Quegan et al., 2019; Dubayah et al., 2020; Johnson et al., 2022). Using repeat aerial LiDAR collections to estimate NSVB AGB growth would be a first step in this direction. Further, direct-change modeling (Healey et al., 2006; Puliti et al., 2021; McRoberts et al., 2015), where estimates of forest structure change (e.g. Δ AGB) between two points in time are made using delta values of remotely sensed imagery (e.g. Δ NDVI), may offer improvements over the stock-change approach implemented here and by Johnson et al. (2023).

4.3. Implications for carbon accounting and management

FIA plot data has been widely used as reference data in model-based approaches to forest carbon mapping and monitoring in the US (e.g, Kennedy et al., 2018a; Johnson et al., 2022, 2023; Huang et al., 2019; Ayrey et al., 2021; Zheng et al., 2007). Given the reported changes associated with NSVB (Westfall et al., 2023), it is perhaps unsurprising that our results show significant differences between NSVB AGB maps and associated estimates and their CRM counterparts. However, we have revealed the potential spatial variability of differences within a state, uncovered challenges with model-based monitoring of NSVB AGB over time, and have confirmed the role of species and size-classes in creating regions of forest carbon gains and losses under a shift to NSVB. In light of these challenges, the spatial distribution of differences, and the general lack of consensus on accounting protocols among carbon markets, there are several potential consequences for spatial forest carbon accounting and related management.

First, NSVB-related shifts may lead to the prioritization of different regions for enrollment in carbon or conservation related programs due to the spatial variability in NSVB-related AGB increases and decreases (Fig. 6). For example, high-elevation regions of the state, where substantial decreases in estimated biomass from CRM to NSVB were concentrated (Section 4.1), could be deprioritized given that other regions may have become more valuable to protect when considering carbon density alone. In a similar vein, managers interested in reforestation for climate-change mitigation potential (Fargione et al., 2018; Johnson et al., 2025) may choose to plant different species or forest-type groups that are estimated to sequester more carbon under a shift to NSVB (e.g. red spruce [*Picea rubens*], eastern hemlock [*Tsuga canadensis*], Fig. 2). Second, the abovementioned challenges in monitoring NSVB AGB growth remotely (Section 4.2) may negatively bias the potential crediting for carbon sequestration in mature forest stands, and to the extent that NSVB-AGB maps and models are used to track progress towards greenhouse gas emissions goals (Lamb et al., 2021), more management or action than necessary may be recommended (Kaarakka et al., 2021; Fargione et al., 2018). Lastly, there may be the opportunity to deliberately choose one system of allometric models over another on a case-by-case basis in order to maximize payments or credits for avoided deforestation, afforestation, or improved management (Gillenwater et al., 2007; Charnley et al., 2010; Kaarakka et al., 2021).

Another factor to consider in the NSVB transition is the accurate conversion of AGB to carbon stocks. NSVB introduced species-specific carbon fractions (Westfall et al., 2023; Doraisami et al., 2022), offering improved AGC accuracy over the 0.5 AGB to AGC ratio assumed with CRM, but at the cost of increased complexity. Under CRM it was standard practice to map AGB and simply convert these initial pixel-level predictions to AGC or belowground carbon (BGC) using fractions that applied to all species (Woodall et al., 2011b; Heath et al., 2009). We followed this standard approach in this study for the sake of comparison to AGB maps produced in Johnson et al. (2023) and only produced estimates of AGC at the state-level using a statewide species-weighted carbon fraction (Section 2.7). However, under NSVB, this AGB-first approach carries the additional requirement of species maps with matching resolution, extent, and general timestamp in order to correctly convert each pixel prediction (Riemann et al., 2014; Wilson et al., 2012, 2013). Alternatively, practitioners may opt to model AGC (or BGC) directly, choosing to incorporate species-specific carbon fractions into reference data at the plot-level. Stand maps, or regional species-group maps, may provide a middle road where pixel-level AGB predictions could be aggregated to stands or regions with approximately known species compositions and more targeted species-weighted carbon ratios could be applied.

4.4. Limitations

We do not suggest that our methods are universal or that our results are nationally conclusive, but rather present this study as a means to explore how the shift to NSVB may impact AGB modeling, mapping, and estimation in general. Further, our analysis is not without assumptions and limitations. There is inherent disagreement between estimates based on our maps and estimates based on FIA's sample, not only with respect to the assumptions underlying design- and model-based inferential frameworks (McRoberts, 2011), but also with regard to both the level of temporal smoothing imposed on the 'temporally indifferent' design-based estimates and the discrepancies in how landcover and landcover change is characterized by each approach (Section 2.4; Bechtold and Patterson (2005); Woodall et al. (2015)). Nonetheless, we use state-level agreement, for both stocks and stock changes as a litmus test for our models and maps. Although estimates of pixel-, plot-, or state-level uncertainty would be required for an operational monitoring system based on NSVB AGB, we omitted them given that the goals of this study were to simply compare top-level results and estimates from NSVB AGB models with those from previously published CRM AGB models. Further research should be dedicated towards understanding how NSVB allometric model error propagates through to estimates of model-based uncertainty (Johnson et al., In review).

5. Conclusion

This study represents a first-of-its-kind investigation into using the new National Scale Volume and Biomass Estimators (NSVB) from the United States (US) Department of Agriculture Forest Inventory and Analysis (FIA) program with existing model-based approaches to map forest aboveground biomass (AGB). Our results suggest that models relying on passive satellite imagery alone (e.g. Landsat) provide acceptable estimates of point-in-time NSVB AGB, but fail to appropriately estimate NSVB AGB accumulation in mature closed-canopy forests. With increasing pressure for forests to sequester carbon and offset greenhouse gas (GHG) emissions from other sectors, models that underpredict or mischaracterize forest growth will not serve to maximize the role forested landscapes will play in natural climate solutions and policies. We highlight that existing maps based on FIA reference data are no longer compatible with NSVB, and recommend incorporating active remote sensing data, retraining models, rethinking AGB to carbon conversions, and updating maps to accommodate this shift.

Indeed, the good practices for GHG inventories outlined by the Intergovernmental Panel on Climate Change (Buendia et al., 2019; Eggleston et al., 2006) describe a mandate ("... greenhouse gas inventories are accurate in a sense that they are systematically neither over- nor underestimates so far as can be judged, and that they are precise so far as practicable") to update our GHG modeling pipelines with improved methods and data streams as they become available. In this instance we have demonstrated that an improvement to one component of a modeling pipeline in isolation (e.g. improved precision and accuracy in reference data) may require rethinking and retooling of other pipeline components. We therefore recommend that model pipelines be revisited holistically, and emphasize the importance of doing so to meet the growing need for accurate spatial forest carbon data that can inform management and decision making across scales.

CRediT authorship contribution statement

Lucas K. Johnson: Writing – original draft, Visualization, Validation, Software, Resources, Methodology, Investigation, Formal analysis, Data curation, Conceptualization. **Michael J. Mahoney:** Writing – original draft, Visualization, Software, Methodology, Data curation, Conceptualization. **Grant M. Domke:** Writing – review & editing, Validation, Conceptualization. **Colin M. Beier:** Writing – review & editing, Supervision, Funding acquisition.

Declaration of competing interest

The authors declare that they have no known competing financial interests or personal relationships that could have appeared to influence the work reported in this paper.

Acknowledgments

We would like to thank the USDA FIA program for their data sharing and cooperation and the NYS Department of Environmental Conservation Office of Climate Change for funding support. The findings and conclusions in this publication are those of the author(s) and should not be construed to represent any official US Department of Agriculture or US Government determination or policy.

Appendix A. Supplementary data

Supplementary material related to this article can be found online at https://doi.org/10.1016/j.foreco.2025.122751.

Data availability

Data will be made available on request.

References

Ayrey, E., Hayes, D.J., Kilbride, J.B., Fraver, S., Kershaw, J.A., Cook, B.D., Weiskittel, A.R., 2021. Synthesizing disparate LiDAR and satellite datasets through deep learning to generate wall-to-wall regional inventories for the complex, mixed-species forests of the eastern United States. Remote. Sens. 13 (24), 5113. http://dx.doi.org/10.3390/rs13245113.

Baston, D., 2022. exactextractr: Fast extraction from raster datasets using polygons. URL: https://CRAN.R-project.org/package=exactextractr, R package version 0.9.1.

Bechtold, W.A., Patterson, P.L., 2005. The Enhanced Forest Inventory and Analysis Program–National Sampling Design and Estimation Procedures, vol. 80, USDA Forest Service, Southern Research Station, URL: https://research.fs.usda.gov/treesearch/20371.

Beven, K.J., Kirkby, M.J., 1979. A physically based, variable contributing area model of basin hydrology / Un modèle à base physique de zone d'appel variable de l'hydrologie du bassin versant. Hydrol. Sci. Bull. 24 (1), 43–69. http://dx.doi.org/10.1080/02626667909491834.

Breiman, L., 2001. Random forests. Mach. Learn. 45 (1), 5–32. http://dx.doi.org/10.1023/a:1010933404324.

Brown, J.F., Tollerud, H.J., Barber, C.P., Zhou, Q., Dwyer, J.L., Vogelmann, J.E., Loveland, T.R., Woodcock, C.E., Stehman, S.V., Zhu, Z., Pengra, B.W., Smith, K., Horton, J.A., Xian, G., Auch, R.F., Sohl, T.L., Sayler, K.L., Gallant, A.L., Zelenak, D., Reker, R.R., Rover, J., 2020. Lessons learned implementing an operational continuous United States national land change monitoring capability: The land change monitoring, assessment, and projection (LCMAP) approach. Remote Sens. Environ. 238, 111356. http://dx.doi.org/10.1016/j.rse.2019.111356.

Buendia, E., Tanabe, K., Kranjc, A., Baasansuren, J., Fukuda, M., Ngarize, S., Osako, A., Pyrozhenko, Y., Shermanau, P., Federici, S., 2019. Refinement to the 2006 IPCC guidelines for national greenhouse gas inventories. IPCC: Geneva, Switz. 5, 194.

CEC, 1997. Ecological Regions of North America: Toward a Common Perspective. Commission for Environmental Cooperation (Montréal, Québec). and Secretariat, URL: https://www.cec.org/files/documents/publications/1701-ecological-regions-north-america-toward-common-perspective-en.pdf.

Charnley, S., Diaz, D., Gosnell, H., 2010. Mitigating climate change through small-scale forestry in the USA: Opportunities and challenges. Small- Scale For. 9 (4), 445–462. http://dx.doi.org/10.1007/s11842-010-9135-x.

Chen, J.M., 1996. Evaluation of vegetation indices and a modified simple ratio for boreal applications. Can. J. Remote Sens. 22 (3), 229–242. http://dx.doi.org/10.1080/07038992.1996.10855178.

Cocke, A.E., Fulé, P.Z., Crouse, J.E., 2005. Comparison of burn severity assessments using differenced normalized burn ratio and ground data. Int. J. Wildland Fire 14, 189–198. http://dx.doi.org/10.1071/WF04010.

Cortes, C., Vapnik, V., 1995. Support-vector networks. Mach. Learn. 20 (3), 273–297. http://dx.doi.org/10.1007/bf00994018.

Deo, R.K., Russell, M.B., Domke, G.M., Woodall, C.W., Falkowski, M.J., Cohen, W.B., 2016. Using landsat time-series and LiDAR to inform aboveground forest biomass baselines in Northern Minnesota, USA. Can. J. Remote Sens. 43 (1), 28–47. http://dx.doi.org/10.1080/07038992.2017.1259556.

Doraisami, M., Kish, R., Paroshy, N.J., Domke, G.M., Thomas, S.C., Martin, A.R., 2022. A global database of woody tissue carbon concentrations. Sci. Data 9 (1), http://dx.doi.org/10.1038/s41597-022-01396-1.

Dormann, C.F., Calabrese, J.M., Guillera-Arroita, G., Matechou, E., Bahn, V., Bartoń, K., Beale, C.M., Ciuti, S., Elith, J., Gerstner, K., Guelat, J., Keil, P., Lahoz-Monfort, J., Pollock, L.J., Reineking, B., Roberts, D.R., Schröder, B., Thuiller, W., Warton, D.I., Wintle, B.A., Wood, S.N., Wüest, R.O., Hartig, F., 2018. Model averaging in ecology: a review of Bayesian, information-theoretic, and tactical approaches for predictive inference. Ecol. Monograph. 88 (4), 485–504. http://dx.doi.org/10.1002/ecm.1309.

Doser, J.W., Stanke, H., Finley, A.O., 2025. rFIA: Estimation of forest variables using the FIA database. URL: https://CRAN.R-project.org/package=rFIA, R package version 1.1.0.

Dubayah, R., Blair, J.B., Goetz, S., Fatoyinbo, L., Hansen, M., Healey, S., Hofton, M., Hurtt, G., Kellner, J., Luthcke, S., Armston, J., Tang, H., Duncanson, L., Hancock, S., Jantz, P., Marselis, S., Patterson, P.L., Qi, W., Silva, C., 2020. The global ecosystem dynamics investigation: High-resolution laser ranging of the Earth's forests and topography. Sci. Remote. Sens. 1, 100002. http://dx.doi.org/10.1016/j.srs.2020.100002.

Duncanson, L., Niemann, K., Wulder, M., 2010. Integration of GLAS and landsat TM data for aboveground biomass estimation. Can. J. Remote Sens. 36 (2), 129–141. http://dx.doi.org/10.5589/m10-037.

Dyer, J.M., 2006. Revisiting the deciduous forests of Eastern North America. BioScience 56 (4), 341–352. http://dx.doi.org/10.1641/0006-3568(2006)56[341:RTDFOE]2.0.CO;2.

Eggleston, H.S., Buendia, L., Miwa, K., Ngara, T., Tanabe, K., 2006. 2006 IPCC guidelines for national greenhouse gas inventories.

Fargione, J.E., Bassett, S., Boucher, T., Bridgham, S.D., Conant, R.T., Cook-Patton, S.C., Ellis, P.W., Falcucci, A., Fourqurean, J.W., Gopalakrishna, T., Gu, H., Henderson, B., Hurteau, M.D., Kroeger, K.D., Kroeger, T., Lark, T.J., Leavitt, S.M., Lomax, G., McDonald, R.I., Megonigal, J.P., Miteva, D.A., Richardson, C.J., Sanderman, J., Shoch, D., Spawn, S.A., Veldman, J.W., Williams, C.A., Woodbury, P.B., Zganjar, C., Baranski, M., Elias, P., Houghton, R.A., Landis, E., McGlynn, E., Schlesinger, W.H., Siikamaki, J.V., Sutton-Grier, A.E., Griscom, B.W., 2018. Natural climate solutions for the United States. Sci. Adv. 4 (11), http://dx.doi.org/10.1126/sciadv.aat1869.

Friedman, J.H., 2002. Stochastic gradient boosting. Comput. Statist. Data Anal. 38 (4), 367–378. http://dx.doi.org/10.1016/s0167-9473(01)00065-2.

Gillenwater, M., Broekhoff, D., Trexler, M., Hyman, J., Fowler, R., 2007. Policing the voluntary carbon market. Nat. Clim. Chang. 1 (711), 85–87. http://dx.doi.org/10.1038/climate.2007.58.

Gray, A., Brandeis, T., Shaw, J., McWilliams, W., Miles, P., 2012. Forest inventory and analysis database of the United States of America (FIA). Biodivers. Ecol. 4, 225–231. http://dx.doi.org/10.7809/b-e.00079.

Hall, R., Skakun, R., Arsenault, E., Case, B., 2006. Modeling forest stand structure attributes using Landsat ETM+ data: Application to mapping of aboveground biomass and stand volume. Forest Ecol. Manag. 225 (1–3), 378–390. http://dx.doi.org/10.1016/j.foreco.2006.01.014.

Healey, S.P., Yang, Z., Cohen, W.B., Pierce, D.J., 2006. Application of two regression-based methods to estimate the effects of partial harvest on forest structure using Landsat data. Remote Sens. Environ. 101 (1), 115–126. http://dx.doi.org/10.1016/j.rse.2005.12.006.

Heath, L.S., Hansen, M.H., Smith, J.E., Smith, W.B., Miles, P.D., 2009. Investigation into calculating tree biomass and carbon in the FIADB using a biomass expansion factor approach. In: McWilliams, W., Moisen, G., Czaplewski, R. (Eds.), 2008 Forest Inventory and Analysis (FIA) Symposium. U.S. Department of Agriculture, Forest Service, Rocky Mountain Research Station, Fort Collins, CO, pp. 21–23, URL: https://research.fs.usda.gov/treesearch/33351.

Hijmans, R.J., 2023. terra: Spatial data analysis. URL: https://rspatial.org/, R package version 1.7-49.

Horvitz, D.G., Thompson, D.J., 1952. A generalization of sampling without replacement from a finite universe. J. Amer. Statist. Assoc. 47 (260), 663–685. http://dx.doi.org/10.1080/01621459.1952.10483446.

Huang, W., Dolan, K., Swatantran, A., Johnson, K., Tang, H., O'Neil-Dunne, J., Dubayah, R., Hurtt, G., 2019. High-resolution mapping of aboveground biomass for forest carbon monitoring system in the Tri-State region of Maryland, Pennsylvania and Delaware, USA. Environ. Res. Lett. 14 (9), 095002. http://dx.doi.org/10.1088/1748-9326/ab2917.

Ji, L., Gallo, K., 2006. An agreement coefficient for image comparison. Photogramm. Eng. Remote Sens. 72 (7), 823–833. http://dx.doi.org/10.14358/pers.72.7.823.

Johnson, L.K., Domke, G.M., Stehman, S.V., Mahoney, M.J., Beier, C.M., From pixels to parcels: flexible, practical small-area uncertainty estimation for spatial averages obtained from aboveground biomass maps, In review, http://dx.doi.org/10.48550/ARXIV.2412.16403.

Johnson, L.K., Mahoney, M.J., Bevilacqua, E., Stehman, S.V., Domke, G.M., Beier, C.M., 2022. Fine-resolution landscape-scale biomass mapping using a spatiotemporal patchwork of LiDAR coverages. Int. J. Appl. Earth Obs. Geoinf. 114, 103059. http://dx.doi.org/10.1016/j.jag.2022.103059.

Johnson, L.K., Mahoney, M.J., Desrochers, M.L., Beier, C.M., 2023. Mapping historical forest biomass for stock-change assessments at parcel to landscape scales. Forest Ecol. Manag. 546, 121348. http://dx.doi.org/10.1016/j.foreco.2023.121348.

Johnson, L.K., Yang, Z., Erb, A., Bright, R.M., Domke, G.M., Frescino, T.S., Schaaf, C.B., Healey, S.P., 2025. Integrating albedo offsets in reforestation decisions for climate change mitigation outcomes in 2050: a case study in the usa. Forest Ecol. Manag. 587, 122699. http://dx.doi.org/10.1016/j.foreco.2025.122699.

Jordan, C.F., 1969. Derivation of leaf-area index from quality of light on the forest floor. Ecology 50 (4), 663–666. http://dx.doi.org/10.2307/1936256.

Kaarakka, L., Cornett, M., Domke, G., Ontl, T., Dee, L.E., 2021. Improved forest management as a natural climate solution: A review. Ecol. Solutions Evid. 2 (3), http://dx.doi.org/10.1002/2688-8319.12090.

Karatzoglou, A., Smola, A., Hornik, K., Zeileis, A., 2004. kernlab – An S4 package for kernel methods in R. J. Stat. Softw. 11 (9), 1–20. http://dx.doi.org/10.18637/jss.v011.i09.

Kauth, R.J., Thomas, G.S.P., 1976. The tasselled cap - a graphic description of the spectral-temporal development of agricultural crops as seen by landsat. In: Symposium on Machine Processing of Remotely Sensed Data. p. 159, URL: https://docs.lib.purdue.edu/cgi/viewcontent.cgi?article=1160&context=lars_symp.

Ke, G., Meng, Q., Finley, T., Wang, T., Chen, W., Ma, W., Ye, Q., Liu, T.-Y., 2017. LightGBM: A highly efficient gradient boosting decision tree. In: Guyon, I., Luxburg, U.V., Bengio, S., Wallach, H., Fergus, R., Vishwanathan, S., Garnett, R. (Eds.), In: Advances in Neural Information Processing Systems, vol. 30, Curran Associates, Inc., URL: https://proceedings.neurips.cc/paper/2017/file/6449f44a102fde848669bdd9eb6b76fa-Paper.pdf.

Kennedy, R.E., Ohmann, J., Gregory, M., Roberts, H., Yang, Z., Bell, D.M., Kane, V., Hughes, M.J., Cohen, W.B., Powell, S., Neeti, N., Larrue, T., Hooper, S., Kane, J., Miller, D.L., Perkins, J., Braaten, J., Seidl, R., 2018a. An empirical, integrated forest biomass monitoring system. Environ. Res. Lett. 13 (2), 025004. http://dx.doi.org/10.1088/1748-9326/aa9d9e.

Kennedy, R.E., Yang, Z., Cohen, W.B., 2010. Detecting trends in forest disturbance and recovery using yearly Landsat time series: 1. LandTrendr — temporal segmentation algorithms. Remote Sens. Environ. 114 (12), 2897–2910. http://dx.doi.org/10.1016/j.rse.2010.07.008.

Kennedy, R.E., Yang, Z., Gorelick, N., Braaten, J., Cavalcante, L., Cohen, W., Healey, S., 2018b. Implementation of the LandTrendr algorithm on Google Earth Engine. Remote. Sens. 10 (5), 691. http://dx.doi.org/10.3390/rs10050691.

Kriegler, F.J., Malila, W.A., Nalepka, R.F., Richardson, W., 1969. Preprocessing Transformations and Their Effects on Multispectral Recognition. In: Remote Sensing of Environment, VI. p. 97, URL: https://ui.adsabs.harvard.edu/abs/1969rse..conf..97K/abstract.

Kuhn, M., Vaughan, D., Hvitfeldt, E., 2023. yardstick: Tidy characterizations of model performance. URL: https://CRAN.R-project.org/package=yardstick, R package version 1.2.0.

Lamb, R.L., Hurtt, G.C., Boudreau, T.J., Campbell, E., Sepúlveda Carlo, E.A., Chu, H.-H., de Mooy, J., Dubayah, R.O., Gonsalves, D., Guy, M., Hultman, N.E., Lehman, S., Leon, B., Lister, A.J., Lynch, C., Ma, L., Martin, C., Robbins, N., Rudee, A., Silva, C.E., Skoglund, C., Tang, H., 2021. Context and future directions for integrating forest carbon into sub-national climate mitigation planning in the RGGI region of the U.S.. Environ. Res. Lett. 16 (6), 063001. http://dx.doi.org/10.1088/1748-9326/abe6c2.

Lorimer, C.G., 2001. Historical and ecological roles of disturbance in Eastern North American forests: 9,000 years of change. Wildl. Soc. Bull. (1973- 2006) 29 (2), 425–439, URL: http://www.jstor.org/stable/3784167.

Lu, D., 2005. Aboveground biomass estimation using Landsat TM data in the Brazilian Amazon. Int. J. Remote Sens. 26 (12), 2509–2525. http://dx.doi.org/10.1080/01431160500142145.

Lu, D., 2006. The potential and challenge of remote sensing-based biomass estimation. Int. J. Remote Sens. 27 (7), 1297–1328. http://dx.doi.org/10.1080/01431160500486732.

Mahoney, M.J., 2023. waywiser: Ergonomic methods for assessing spatial models. http://dx.doi.org/10.48550/arXiv.2303.11312.

Mahoney, M.J., Beier, C.M., Ackerman, A.C., 2022a. terrainr: An R package for creating immersive virtual environments. J. Open Source Softw. 7 (69), 4060. http://dx.doi.org/10.21105/joss.04060.

Mahoney, M.J., Johnson, L.K., Guinan, A.Z., Beier, C.M., 2022b. Classification and mapping of low-statured shrubland cover types in post-agricultural landscapes of the US northeast. Int. J. Remote Sens. 43 (19–24), 7117–7138. http://dx.doi.org/10.1080/01431161.2022.2155086.

Massey, Jr., F.J., 1951. The Kolmogorov-Smirnov test for goodness of fit. J. Amer. Statist. Assoc. 68–78. http://dx.doi.org/10.2307/2280095.

McRoberts, R.E., 2011. Satellite image-based maps: Scientific inference or pretty pictures? Remote Sens. Environ. 115 (2), 715–724. http://dx.doi.org/10.1016/j.rse.2010.10.013.

McRoberts, R.E., Næsset, E., Gobakken, T., Bollandsås, O.M., 2015. Indirect and direct estimation of forest biomass change using forest inventory and airborne laser scanning data. Remote Sens. Environ. 164, 36–42. http://dx.doi.org/10.1016/j.rse.2015.02.018.

Miles, P.D., 2015. Batch reporting of forest inventory statistics using the evalidator. In: Stanton, Sharon M.; Christensen, Glenn A., Comps. 2015. Pushing Boundaries: New Directions in Inventory Techniques and Applications: Forest Inventory and Analysis (FIA) Symposium 2015. 2015 December 8–10; Portland, Oregon. Gen. Tech. Rep. PNW-GTR-931. Portland, OR: US Department of Agriculture, Forest Service, Pacific Northwest Research Station: 78-83, vol. 931, pp. 78–83.

Montero, D., Aybar, C., Mahecha, M.D., Wieneke, S., 2022. Spectral: Awesome spectral indices deployed via the Google earth engine Javascript API. Int. Arch. Photogramm. Remote. Sens. Spat. Inf. Sci. XLVIII-4/W1-2022, 301–306. http://dx.doi.org/10.5194/isprs-archives-xlviii-4-w1-2022-301-2022.

NOAA National Centers for Environmental Information, 2022. Climate at a glance: Statewide mapping. https://www.ncdc.noaa.gov/cag/. (Accessed: 23 January 2022).

Omernik, J.M., Griffith, G.E., 2014. Ecoregions of the conterminous United States: Evolution of a hierarchical spatial framework. Environ. Manag. 54 (6), 1249–1266. http://dx.doi.org/10.1007/s00267-014-0364-1.

Pflugmacher, D., Cohen, W.B., E. Kennedy, R., 2012. Using landsat-derived disturbance history (1972–2010) to predict current forest structure. Remote Sens. Environ. 122, 146–165. http://dx.doi.org/10.1016/j.rse.2011.09.025.

Powell, S.L., Cohen, W.B., Healey, S.P., Kennedy, R.E., Moisen, G.G., Pierce, K.B., Ohmann, J.L., 2010. Quantification of live aboveground forest biomass dynamics with landsat time-series and field inventory data: A comparison of empirical modeling approaches. Remote Sens. Environ. 114 (5), 1053–1068. http://dx.doi.org/10.1016/j.rse.2009.12.018.

PRISM Climate Group, 2022. PRISM climate data. https://prism.oregonstate.edu. (Accessed: 20 January 2022).

Pugh, S.A., Turner, J.A., Burrill, E.A., David, W., 2018. The forest inventory and analysis database: Population estimation user guide. URL: https://research.fs.usda.gov/sites/default/files/2024-05/wo-nov2018_ug_population_estimation.pdf.

Puliti, S., Breidenbach, J., Schumacher, J., Hauglin, M., Klingenberg, T.F., Astrup, R., 2021. Above-ground biomass change estimation using national forest inventory data with Sentinel-2 and Landsat. Remote Sens. Environ. 265, 112644. http://dx.doi.org/10.1016/j.rse.2021.112644.

Quegan, S., Le Toan, T., Chave, J., Dall, J., Exbrayat, J.-F., Minh, D.H.T., Lomas, M., D'Alessandro, M.M., Paillou, P., Papathanassiou, K., Rocca, F., Saatchi, S., Scipal, K., Shugart, H., Smallman, T.L., Soja, M.J., Tebaldini, S., Ulander, L., Villard, L., Williams, M., 2019. The European Space Agency BIOMASS mission: Measuring forest above-ground biomass from space. Remote Sens. Environ. 227, 44–60. http://dx.doi.org/10.1016/j.rse.2019.03.032.

R Core Team, 2023. R: A Language and Environment for Statistical Computing. R Foundation for Statistical Computing, Vienna, Austria, URL: https://www.R-project.org/.

Riemann, R.I., Wilson, B.T., Lister, A.J., Cook, O., Crane-Murdoch, S., 2014. Modeled Distributions of 12 Tree Species in New York. U.S. Department of Agriculture, Forest Service, Northern Research Station, http://dx.doi.org/10.2737/nrs-rmap-5.

Riemann, R.I., Wilson, B.T., Lister, A., Parks, S., 2010. An effective assessment protocol for continuous geospatial datasets of forest characteristics using USFS forest inventory and analysis (FIA) data. Remote Sens. Environ. 114 (10), 2337–2352. http://dx.doi.org/10.1016/j.rse.2010.05.010.

Roy, D., Kovalskyy, V., Zhang, H., Vermote, E., Yan, L., Kumar, S., Egorov, A., 2016. Characterization of Landsat-7 to Landsat-8 reflective wavelength and normalized difference vegetation index continuity. Remote Sens. Environ. 185, 57–70. http://dx.doi.org/10.1016/j.rse.2015.12.024.

Shi, Y., Ke, G., Soukhavong, D., Lamb, J., Meng, Q., Finley, T., Wang, T., Chen, W., Ma, W., Ye, Q., Liu, T.-Y., Titov, N., Cortes, D., 2022. lightgbm: Light gradient boosting machine. URL: https://github.com/Microsoft/LightGBM, R package version 3.3.2.99.

Simard, M., Pinto, N., Fisher, J.B., Baccini, A., 2011. Mapping forest canopy height globally with spaceborne lidar. J. Geophys. Res. 116 (G4), http://dx.doi.org/10.1029/2011jg001708.

Stanke, H., Finley, A.O., Weed, A.S., Walters, B.F., Domke, G.M., 2020. rFIA: An R package for estimation of forest attributes with the US forest inventory and analysis database. Environ. Model. Softw. 127, 104664. http://dx.doi.org/10.1016/j.envsoft.2020.104664.

Stehman, S.V., Foody, G.M., 2019. Key issues in rigorous accuracy assessment of land cover products. Remote Sens. Environ. 231, 111199. http://dx.doi.org/10.1016/j.rse.2019.05.018.

US Census Bureau, 2013. TIGER/Line shapefiles. URL: https://www.census.gov/geographies/mapping-files/time-series/geo/tiger-line-file.html.

US Geological Survey, 2019. 3D elevation program 1-meter resolution digital elevation model. https://www.usgs.gov/the-national-map-data-delivery. (Accessed: 20 January 2022).

USGS, 2018. Landsat Collections. US Geological Survey, http://dx.doi.org/10.3133/fs20183049.

Virginia Tech, 2023a. Overview of the national scale volume and biomass estimators (NSVB): State report for Indiana. Archived at https://web.archive.org/web/20231221224951/https://charcoal2.cnre.vt.edu/nsvb_factsheets/Reports/State/Indiana.html, https://charcoal2.cnre.vt.edu/nsvb_factsheets/Reports/State/Indiana.html. (Accessed: 21 December 2023).

Virginia Tech, 2023b. Overview of the national scale volume and biomass estimators (NSVB): State report for new york. Archived at https://web.archive.org/web/20231009182935/https://charcoal2.cnre.vt.edu/nsvb_factsheets/Reports/State/New York.html, https://charcoal2.cnre.vt.edu/nsvb_factsheets/Reports/State/New York.html, (Accessed: 09 October 2023).

Virginia Tech, 2023c. Overview of the national scale volume and biomass estimators (NSVB): State report for washington. Archived at https://web.archive.org/web/20231221225113/https://charcoal2.cnre.vt.edu/nsvb_factsheets/Reports/State/Washington.html, https://charcoal2.cnre.vt.edu/nsvb_factsheets/Reports/State/Washington.html. (Accessed: 21 December 2023).

Walker, K., 2023. tigris: Load census TIGER/Line shapefiles. URL: https://CRAN.R-project.org/package=tigris, R package version 2.0.3.

Westfall, J.A., Coulston, J.W., Gray, A.N., Shaw, J.D., Radtke, P.J., Walker, D.M., Weiskittel, A.R., MacFarlane, D.W., Affleck, D.L., Zhao, D., Temesgen, H., Poudel, K.P., Frank, J.M., Prisley, S.P., Wang, Y., Meador, A.J.S., Auty, D., Domke, G.M., 2023. A National-Scale Tree Volume, Biomass, and Carbon Modeling System for the United States. U.S. Department of Agriculture, Forest Service, http://dx.doi.org/10.2737/wo-gtr-104.

Whitney, G.G., 1994. From Coastal Wilderness to Fruited Plain: A History of Environmental Change in Temperate North America from 1500 to the Present. Cambridge University Press.

Wilson, B.T., Lister, A.J., Riemann, R.I., 2012. A nearest-neighbor imputation approach to mapping tree species over large areas using forest inventory plots and moderate resolution raster data. Forest Ecol. Manag. 271, 182–198. http://dx.doi.org/10.1016/j.foreco.2012.02.002.

Wilson, B.T., Lister, A.J., Riemann, R.I., Griffith, D.M., 2013. Live tree species basal area of the contiguous United States (2000–2009). For. Serv. Res. Data Arch. http://dx.doi.org/10.2737/rds-2013-0013.

Wolpert, D.H., 1992. Stacked generalization. Neural Netw. 5 (2), 241–259. http://dx.doi.org/10.1016/s0893-6080(05)80023-1.

Woodall, C.W., Coulston, J.W., Domke, G.M., Walters, B.F., Wear, D.N., Smith, J.E., Andersen, H.-E., Clough, B.J., Cohen, W.B., Griffith, D.M., Hagen, S.C., Hanou, I.S., Nichols, M.C., Perry, C.H.H., Russell, M.B., Westfall, J., Wilson, B.T.T., 2015. The U.S. Forest Carbon Accounting Framework: Stocks and Stock Change, 1990–2016. U.S. Department of Agriculture, Forest Service, Northern Research Station, http://dx.doi.org/10.2737/nrs-gtr-154.

Woodall, C.W., Domke, G.M., Macfarlane, D.W., Oswalt, C.M., 2011a. Comparing field- and model-based standing dead tree carbon stock estimates across forests of the US. Forestry 85 (1), 125–133. http://dx.doi.org/10.1093/forestry/cpr065.

Woodall, C.W., Heath, L.S., Domke, G.M., Nichols, M.C., 2011b. Methods and Equations for Estimating Aboveground Volume, Biomass, and Carbon for Trees in the U.S. Forest Inventory, 2010. Technical Report, U.S. Department of Agriculture, Forest Service, Northern Research Station, http://dx.doi.org/10.2737/nrs-gtr-88.

Wright, M.N., Ziegler, A., 2017. **ranger**: A fast implementation of random forests for high dimensional data in *C++* and *R*. J. Stat. Softw. 77 (1), http://dx.doi.org/10.18637/jss.v077.i01.

Zheng, D., Heath, L.S., Ducey, M.J., 2007. Forest biomass estimated from MODIS and FIA data in the Lake States: MN, WI and MI, USA. Forestry 80 (3), 265–278. http://dx.doi.org/10.1093/forestry/cpm015.

Zhu, Z., Woodcock, C.E., 2014. Continuous change detection and classification of land cover using all available landsat data. Remote Sens. Environ. 144, 152–171. http://dx.doi.org/10.1016/j.rse.2014.01.011.